ABSTRACT

Title of dissertation: MORPHOLOGICAL INSTABILITIES AND STEP PATTERN FORMATION ON VICINAL SURFACES

Tong Zhao, Doctor of Philosophy, 2004

Dissertation directed by: Professor John D. Weeks
Institute for Physical Science and Technology
Department of Chemistry

Vicinal surfaces can exhibit a number of different instabilities and step pattern formation that are important in directed growth and nanofabrication. This dissertation attempts to present some theoretical progress made in understanding and predicting the evolution of surface morphology under direct current heating.

We study current-induced instabilities found on both Si(111) and Si(001) surfaces with a physically suggestive two-region diffusion model, motivated by the idea of surface reconstruction or rebonding that often occurs on semiconductor surfaces. The model not only gives a coherent and unified view of the seemingly different instabilities on both surfaces, but also provides a physical way of interpreting the boundary conditions in classic sharp step models. In particular, we find that the effective kinetic coefficient can be negative.

The studies of instabilities enlighten us to pursue a systematic study of the general linear kinetics boundary conditions in sharp step models. We construct a one dimensional discrete hopping model that takes into account both the asymmetry in the hopping rates near a step and the finite probability of incorporation into the solid at the step site. By appropriate extrapolation, we relate the kinetic coefficient and permeability rate in general sharp step models to the physically suggestive

parameters of the hopping models. The derivation shows in general the kinetic rate parameters can be negative when diffusion is faster near the step than on terraces.

The subsequent step pattern formation resulting from current-induced instabilities are also discussed. The velocity function formalism is applied to step bunching and in-phase wandering. The more intricate step wandering patterns are treated by a nonlinear evolution equation derived from a geometric representation of the two dimensional curves. The results from numerical calculations resemble the patterns observed in experiments. Two dimensional kinetic Monte Carlo simulations are implemented in a qualitative way, with an emphasis on the physical realization of the effective boundary conditions in terms of microscopic hopping rates. The simulations confirm both the theory of current-induced instabilities and the derivation of boundary conditions.

MORPHOLOGICAL INSTABILITIES AND STEP PATTERN FORMATION ON VICINAL SURFACES

by

Tong Zhao

Dissertation submitted to the Faculty of the Graduate School of the
University of Maryland, College Park in partial fulfillment
of the requirements for the degree of
Doctor of Philosophy
2004

Advisory Committee:

Professor John D. Weeks, Chair/Advisor
Professor Theodore L. Einstein
Professor Ellen D. Williams
Professor Janice Reutt-Robey
Professor Eitan Tadmor

© Copyright by
Tong Zhao
2004

DEDICATION

To my family and to the past six memorable years in Maryland.

ACKNOWLEDGMENTS

First and foremost of all I would like to thank my advisor, Professor John D. Weeks who provided me with such an invaluable opportunity to work under his guidance. The past four years has been a great, and perhaps the most important learning experience in my life. From him I have learned how to tackle real problems instead of homework, how to bring forth the physical principles in a as clean as possible way, and how to express them succinctly and clearly in a scientific paper or presentation. During the four years, his door has always been open to me for discussions or advice and his amiable personality has made it such a pleasure to learn from and work with him. Both his profound insights into the subject and his kindness to others will have a far reaching influence in my career and in my life.

I feel extremely grateful to Dr. Daniel Kandel, with whom we have extensive and stimulating discussions during his visit last summer. Some of the discussions have directly led to useful results that are included in this thesis. I also owe my gratitude to Professor Janice Reutt-Robey, who introduced me to the surface field and supported me during the first summer I was here. I thank Professor Theodore L. Einstein and Professor Ellen D. Williams for critical reading on my manuscripts including this thesis and making constructive suggestions. Thanks are also due to Professor Eitan Tadmor for spending his time serving as dean's representative in the committee and reviewing the thesis. Professor Michael A. Coplan can not be left out here. As the program director, he helped me greatly in the early days of my graduate life.

I would also like to express my gratitude to all the members in the groups of Professor Weeks, Professor Einstein, and Professor Williams. I benefited enormously from those group meetings and lunch discussions that we have had over the years.

Finally, there are all the administrative staff in the chemical physics program and MRSEC. Ms. Diane Mancuso and Ms. Shirley Winter in particular were always cheerful guides in going through the drudgeries of the university and departmental maze of paperwork.

TABLE OF CONTENTS

Chapter 1

Introduction

1.1 Overview

The main purpose of this dissertation is to develop theoretical understanding of the evolution of surface morphology at length scales from nanometers to microns. First of all, a wealth of experimental data that could lead to an understanding at these length scales has become available with the development of powerful microscopic probing techniques, such scanning tunneling microscopy (STM), which essentially allow the observation of atomic structures on crystal surfaces. More importantly, the forefront of current research is focused on developing novel materials and device properties in these length scales. The combination of the two have greatly inspired the study of fundamental physics on crystal surfaces. One of the interesting subjects is to study the morphological instabilities and evolution under various external driving fields (eg. growth, etching and electric current), since the patterns generated may provide useful templates for nanoscale fabrication.

In particular, this dissertation centers around the instabilities and morphological evolutions on silicon surfaces with a particular driving field - a direct electric current. This problem is of great interest not only because it serves as a physical example of pattern formation on a length scale of interest in a system driven

far from equilibrium by a weak and controllable field, but also because it provides a unique and experimentally controllable probe that can uncover many aspects of fundamental physics on crystal surfaces.

The dissertation is structured as the following. In this first chapter, the thermodynamics of vicinal surfaces are briefly reviewed to provide a necessary background. An overview of step dynamics as a moving boundary problem follows, to introduce some general idea of instabilities and boundary conditions that will be the main focus in the rest of the dissertation.

In Chapter 2 and 3, we study in detail of the physical origins of current-induced instabilities on both Si(111) and Si(001) surfaces, and provide a coherent and unified view of current-induced instabilities. The results from these studies point to the importance and necessity of further understanding on the general boundary conditions for modeling step dynamics. We pursue this general problem in Chapter 4 with a physically instructive hopping model, that relates the "microscopic" parameters in kinetic Monte Carlo simulations to the effective parameters in continuum boundary conditions.

Having understood the instabilities and related issue of boundary conditions, in Chapter 5 we study the interesting step pattern formations as the results of the current-induced instabilities. Three different approaches - velocity function integration, geometric formulation and kinetic Monte Carlo simulation will be discussed.

Finally, some concluding remarks are given in Chapter 6.

1.2 Surface Morphology and Representation

A surface is a boundary between two macroscopic regions with different phases. For the surfaces of primary interest in this thesis, one of the phases is a crystalline solid.

In order to create such a surface, one has to break chemical bonds, and this costs energy. At finite temperature, it is more appropriate to consider free energy. One can think of breaking a crystalline material along a plane. The process results in two surfaces with equal area S, and it requires a certain amount of work W. The surface free energy per unit area or surface tension is defined as $\sigma \equiv W/(2S)$.

Usually the solid phase is anisotropic, and thus the surface tension σ depends on surface orientation. At low temperatures, crystallographic orientations of high symmetry (low Miller index) generally represent local minima in the surface free energy. The surfaces misoriented at small angles to such high symmetry planes are called *vicinal* surfaces, which consist of *terraces* at high symmetry orientation separated by *steps* of atomic-layer height. It is often useful to define the surface free energy per unit projected area $f(\theta, T) \equiv \sigma(\theta, T)/\cos\theta$ in the high symmetry plane, where θ is the misorientation angle and T is temperature. When the angle is small and the step density is low, the reduced free energy density takes the form [1, 2]

$$f(\theta, T) = f_0(T) + \frac{\beta(T)}{h}|\tan\theta| + \frac{g}{h^3}|\tan\theta|^3. \tag{1.1}$$

The first term $f_0(T) = \sigma(0, T)$ is the surface free energy per unit area of the high symmetry plane. The second term represents the step free energy contribution, in which $\beta(T)$ is the free energy per unit length for forming an isolated single-layer height (denoted as h) step and $|\tan\theta|/h$ is the step density. The last term is due to interactions between steps and g is a parameter that depends on the step stiffness (to be defined in next section), temperature and specific type of interaction [3].

It is easy to see from Eq. (1.1) that the surface free energy has a cusp singularity at the orientation of the high symmetry plane. At high enough temperatures where excitations on terraces occur, it is known that the step free energy will eventually vanish and the surface becomes rough since its free energy has minima at nonvanishing step densities. This corresponds to a well-studied phase transition - often called roughening transition [4, 5], and the exact temperature at which the

step free energy vanishes is called the roughening temperature (T_R). The roughening transition of the high symmetry surface occurs below the melting point ($T_R < T_M$), and is a very weak transition in the sense that the theoretical result from renormalization group calculations shows [4, 5, 6] that

$$\beta(T) \sim \exp\left[-\sqrt{\frac{T_1}{T_R - T}}\right], \tag{1.2}$$

where T_1 is a constant.

Above T_R, fluctuations are sufficiently strong that the discreteness of the crystal lattice becomes negligible, so that the surface may be represented by a continuum height function $z(x, y)$ in Cartesian coordinates. The surface tension is then a function of the partial derivatives $z_x = \partial z/\partial x$ and $z_y = \partial z/\partial y$. The total surface free energy at a given temperature is simply

$$\mathcal{F} = \iint \sigma(z_x, z_y)\sqrt{1 + z_x^2 + z_y^2}dxdy = \iint f(z_x, z_y)\,dxdy. \tag{1.3}$$

Throughout the thesis, the surfaces of interest are vicinal surfaces that are well below T_R of the corresponding high symmetry plane. The morphology of such surfaces is governed by the behavior of discrete steps. From the above discussion, one can see that it is appropriate to incorporate this discreteness in the surface representation at temperatures below T_R. However, it turns out possible (see discussion in the next section) to maintain much of the computational simplicity of a continuum approach by treating the step as a continuum string-like entity. Therefore, the surface is characterized by $x_n(y)$, where $n = 1, 2, ...$ is the step index and y is the continuum dimension along the step. The surface free energy is thus a functional of $x_n(y)$, which can be written as a sum of the energies of individual steps and their interactions

$$\mathcal{F}(\{x_n(y)\}) = \int dy \sum_n \left[\beta(\phi) + V(\{w_n(y)\})\right], \tag{1.4}$$

where ϕ is the angle characterizing local step direction, which is a function of $x_n'(y)$ in Cartesian coordinates (prime here denotes derivative with respect to y). V is effective step interaction that depends on step separations $W_n(y)$.

1.3 Thermodynamics of Vicinal Steps

The thermodynamic properties of a single step are contained in $\beta(\phi)$ — the step free energy per unit length. However, to further investigate $\beta(\phi)$, one has to think about whether there is a similar roughening transition for a one dimensional step as for two dimensional surfaces. The answer is that the step is always rough at any finite temperature, which justifies the validity of the continuum description on this dimension in the previous section. The reason lies in the fact that the creation of a *kink* (taking one atom out of the straight step creates two kinks) on a one dimensional step requires only a fixed small energy cost. Once one such kink has formed neighboring kinks can be very easily excited. Thus there is a finite kink density at any temperatures above zero, and step fluctuations are easily excited.

1.3.1 An Isolated Step - Chemical Potential and Stiffness

At any finite temperature, the free energy for an isolated step can be conveniently written as a continuum integral in terms of geometrical quantities

$$F = \int ds\beta(\phi), \tag{1.5}$$

where s denotes the arc length along the step. The *step chemical potential*, defined as the free energy change upon adding an atom to the step, can be obtained by taking the derivative of F with respect to a virtual displacement $\delta\xi$ of the step position

$$\mu = \Omega\frac{\delta F}{\delta\xi} = \Omega\widetilde{\beta}\kappa, \tag{1.6}$$

in which $\widetilde{\beta}$ is commonly called *step stiffness* that has the form related to the step free energy

$$\widetilde{\beta} \equiv \beta + \frac{\partial^2\beta}{\partial\phi^2} \tag{1.7}$$

and $\kappa \equiv \partial\phi/\partial s$ is the local step curvature.

Finally, it is straightforward to derive Eqs. (1.5-1.7) using Cartesian coordinates in accord with Eq. (1.4). When the step fluctuations are small ($x'(y) \ll 1$), this yields

$$F = \int dy \frac{\widetilde{\beta}}{2} \left[\frac{\partial x}{\partial y}\right]^2 \tag{1.8}$$

and the linearized chemical potential $\mu = \Omega\widetilde{\beta}\partial^2 x/\partial y^2$.

1.3.2 A Step Array — Step-Step Repulsions

Eq. (1.6) only applies to an isolated step. It is more of interest to determine the step chemical potential in a step array, which will be modified by step-step interactions ($V(\{w_n(y)\})$ in Eq. (1.4)). The most evident interaction between steps is the step-step repulsion induced by the configurational entropy. The transverse fluctuations of a step tend to be suppressed by its neighbors due to the prohibitively high energy cost associated with step crossings and overhangs. This produces an effective repulsion between steps that favors uniform step spacing at equilibrium. Clearly the repulsive interaction between steps depends on the step separation. It was shown by Gruber and Mullins [1] that the interaction is proportional to $1/w^2$, where w is the average step separation in the uniform step array. Other types of interactions exist, such as elastic [7, 8] or dipole interactions [9], which generally give rise to the same inverse square dependence on step separations.

Assuming only nearest- neighbor interactions, the step interaction term in Eq. (1.4) can be effectively treated as

$$V(\{w_n(y)\}) = g/w_n^2(y), \tag{1.9}$$

where g is some constant and $w_n(y) \equiv x_{n+1}(y) - x_n(y)$ is the local terrace width.

Therefore, the step chemical potential in a step array is given by

$$\mu_n = \mu + 2g \left[\frac{1}{w_{n-1}^3(y)} - \frac{1}{w_n^3(y)} \right], \tag{1.10}$$

in which μ is the isolated step chemical potential given by Eq. (1.6).

1.4 Step Dynamics - Boundary Conditions and Instabilities

In many interesting practical processes including crystal growth [10], etching [11] and surface electromigration [12], the vicinal surface is driven far from equilibrium. Typically, there is a non uniform adatom (atoms adsorbed on surfaces) concentration field $c(x, y, t)$ on each terrace. The steps are boundaries separating the concentration fields on neighboring terraces. The steps serve as sources and sinks of adatoms, and evolve in time by exchanging mass with the terrace concentration fields. Hence the step dynamics belongs to the class of moving boundary problems. The formulation of step dynamics generally requires consideration of both the dynamics of the adatom concentration field and the appropriate boundary conditions at steps. While the adatom concentration field can be treated quite straightforwardly in most cases, the appropriate formulation of boundary conditions can be very subtle, since it inevitably involves assumptions about the underlying microscopic physics. In fact, the interplay between the external driving force and step boundary conditions constitutes the major theme in the studies of dynamic modeling of vicinal steps.

This interplay often results in kinetic instabilities. Two types of step instabilities are commonly seen on vicinal surfaces. One is *step bunching* - steps are closely packed and separated by wide terraces, which is essentially a one dimensional instability. The other is *step wandering* - steps undergo long wavelength undulations, which requires a two dimensional treatment of the step.

It is well known that the general solution of the moving boundary problem as described above is a formidable challenge [13, 14]. For this reason, the problem is usually formulated using the *quasi-static* approximation. As will be discussed in detail later, this assumes that the terrace concentration field relaxes faster that the typical time scale for step motion. Thus the terrace concentration field can be first determined for fixed step positions. This is very similar to the Born-Oppenheimer approximation in quantum mechanics, which separates the different time scales for electronic and nuclear motion. Using this approximation, the instabilities can be analyzed by linear stability analyses on fairly simple surface morphologies corresponding to the steady states, and the subsequent surface morphology can be carried out by numerical integration.

Chapter 2

Current-Induced Instabilities on Vicinal Si(111) Surfaces

2.1 Electromigration Experiments on Vicinal Si(111) Surfaces

Electromigration refers to the enhanced diffusion of atoms in response to an applied electric field. This phenomenon has long been of great scientific and technological interest, particularly in metals, since it represents the failure mode of many microelectronic devices [15, 16]. Researchers have also studied *surface electromigration*, the enhanced motion of adatoms on a surface in response to an applied field. In particular, current induced instabilities on vicinal Si(111) surfaces have received a great deal of attention since the first experiments were carried out by Latyshev *et al.* in 1989 [17]. They observed the formation of closely packed step bunches separated by wide step-free terraces after a vicinal surface with monatomic height and equidistant steps is resistively heated with a properly directed direct electric current. The uniform step train is stable when the current flows in the opposite direction. Since then, current induced step bunching on Si(111) surfaces have been studied by several

research groups using various modern microscopy techniques (AFM, REM, STM, synchrotron X-ray scattering, etc.) [18, 19, 20, 21, 22, 23, 24, 25, 26]. These experiments show clearly that the instabilities can manifest themselves with different characteristic step patterns.

Moreover they show that the bunching instability has a mysterious dependence on temperature. At temperatures between the first-order phase transition ($T_c \cong$ 830°C) [27, 28] between the 7×7 and 1×1 reconstructed surface and about 1050°C (we shall call this range I), the bunching instability occurs with a step-down direction of current. At higher temperatures, in the range of 1050°C−1150°C (range II), the direction of current causing the bunching instability reverses. Surprisingly, above 1150°C (range III) it changes back again to the step-down direction. Moreover, recent experiments [29, 30, 31] have revealed that the step train in range II under a step-down current, originally thought to be completely regular and stable, undergoes a novel in-phase *wandering instability* after being heated for a longer time.

2.2 Theoretical Development

The first quantitative treatment of step flow on crystal surface was carried out by Burton, Cabrera and Frank [32] more that fifty years ago. They assumed that the rate limiting step for mass transfer on vicinal surfaces arises from adatom diffusion on the terraces. Steps at the boundaries of terraces were assumed to act as perfect sinks or sources for adatoms so that local equilibrium at the step edges is always maintained. Since then, many authors have offered various generalizations and clarifications of the BCF theory. Perhaps the most significant modification is to account for the deviation from local equilibrium arising from the finite adatom attachment/detachment rate at both edges of the step. This is indeed necessary for materials such as semiconductors where the mass exchange between steps and terrace edges is not fast enough to maintain local equilibrium.

In important work Stoyanov [33, 34] first extended the BCF theory to describe electromigration on vicinal Si(111) surfaces. He proposed that each surface adatom acquires an *effective charge* z^* and thus feels a constant force (the electromigration force, usually written as $\mathbf{F} = z^* e\mathbf{E}$) from the electric field. The adatoms thus undergo *driven diffusion* in the presence on an electric field. Within this general mathematical framework a number of researchers have proposed different physical mechanisms to account for particular aspects of this mysterious phenomenon. In particular, two main theories have been suggested to explain the existence of electromigration instabilities, as well as the change in the stable and unstable current directions.

1. *Attachment/detachment limited kinetics in all temperature regimes arising from step reconstruction along with a change of sign of the effective charge* [35, 36]. This idea is motivated by the physics of rebonding and surface reconstruction that can occur near steps as the system tries to minimize the excess free energy associated with "broken bonds" at the step edge. The step reconstruction gives rise to an energy barrier to incorporate an additional adatom into the step, since it requires a collective motion of many atoms as the rebonding is modified. In presence of this barrier, it was shown that the direct current will always induce a bunching instability if it is in the same direction as the electromigration force, and will stabilize the uniform step train if it is in the opposite direction. Thus, the unstable current direction will change provided that the sign of the effective charge on adatoms changes [36] in the three temperature ranges. The barrier is an essential feature here; if the step is assumed to be in local equilibrium, then the bunching instability is not found. This theory is successful in understanding fundamental bunching dynamics as well as related experiments, such as 2D step patterning [37] and anti-band formation [38]. However, it has difficulty in explaining in-phase wandering in temperature range II. Moreover, experimental evidence seems to suggest that the sign of the effective charge stays positive for all three temperature ranges [39].

2. *Significant step transparency in temperature range II with the same positive effective charge* [40, 41]. Some researchers attributed the change of the unstable current direction to a change in step transparency associated with different kink densities. They assume that unlike the other two ranges, the kink densities are especially low in temperature range II, so that the adatoms are most likely to cross the step without being solidified at kinks. However, there are at least two important physical aspects that this theory did not make clear. First, it is not obvious why the kink densities should change non-monotonically with temperature. Second, even if the kink density were lower, still it is hard to understand physically why the nearly uniform surface diffusion (except at the very few kink sites where the communication between crystal solid and surface adatoms takes place in the normal way) could generate any instabilities.

Some other scenarios have also been suggested. Suga *et al.* [42] proposed field-dependent kinetic coefficients based on a series of simulation models. In their model both step bunching and wandering instabilities are obtained in temperature range II with the same positive effective charge, when the kinetic processes associated with steps become much faster compared to terrace diffusion. The theory is not as widely accepted as the other two. In fact, we will show in Chapter 4 that the kinetic coefficients are independent of the field under typical experimental conditions where the field is very weak. However, their simulations suggest the possibility of diffusion limited kinetics in temperature range II as apposed to attachment/detachment limited in the previous two theories, which in part motivates the work below.

2.3 A Two-Region Diffusion Model

It is well known that the dangling bonds at semiconductor surfaces quite generally rearrange to form characteristic surface reconstructions. We expect a different local rearrangement of bonds in the vicinity of a step, which itself represents an additional

source of dangling bonds. Clearly this reconstruction can directly influence surface mass transport and hence possible instabilities. Standard boundary conditions in the continuum sharp step model may include some effects of surface reconstruction in special cases. For example, Liu and Weeks [35] interpreted electromigration experiments in the lowest temperature regime of Si(111) using attachment/detachment limited kinetics, and argued that the attachment barriers could arise from a local reconstruction of the dangling bonds at a step edge. However, it is not clear how this picture should be modified at higher temperatures.

Steps differ fundamentally from terraces by serving as sources and sinks for adatoms. In the classical BCF picture it was assumed that the local equilibrium concentration of adatoms at a step is maintained even in the presence of non equilibrium driving forces. In addition the rates of various mass transport processes near steps can differ from kinetic processes on terraces, e.g., because of differences in local surface reconstructions. The kinetic coefficients in generalized BCF models try to take both features of steps into account in an effective way.

Our approach here is to consider a more detailed description where both features are treated separately in the simplest possible way. We then obtain the relevant sharp step boundary condition by an appropriate coarse-graining. To that end, we assume that an atomic step has sufficient kink sites to maintain a local equilibrium concentration of adatoms as in the classical BCF picture. Reconstruction is taken into account by assuming that the atomic step is surrounded by a *step region* where adatoms undergo effective diffusion with a diffusion constant D_s that can differ from D_t, the value found on terraces.

Here we use the simplest realization of this idea, where the reconstruction is assumed to occur fast relative to step motion, so that the step region moves with the atomic step and has a fixed width s of a few lattice spacings at a given temperature. Thus a uniform vicinal surface can be viewed as an array of repetitive two-region units, made up of the step region and its neighboring lower terrace re-

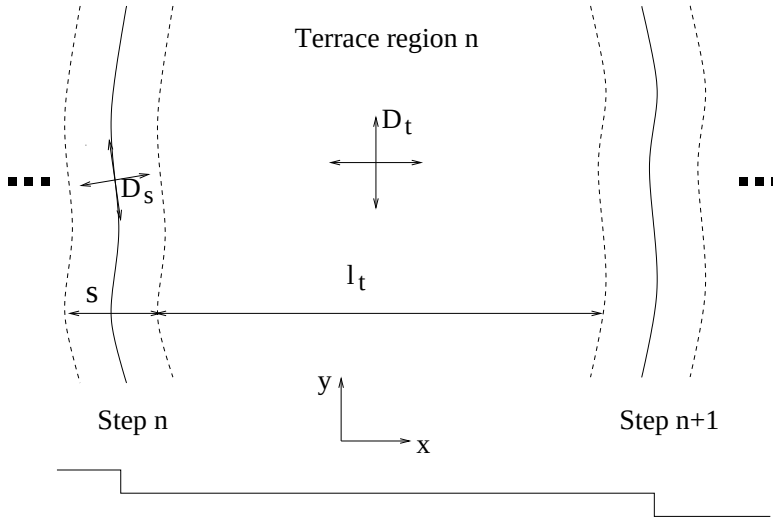

Figure 2.1: The upper part of the figure shows a 2D schematic view of the vicinal surface composed of different reconstruction regions on terraces and near steps, separated by dashed lines. In this paper, we assume that the step reconstruction with a fixed width s always follows the motion of the atomic step (solid line). The lower part of the figure shows a corresponding 1D side view that illustrates our coordinate system.

gion. We assume that straight steps extend along the y direction and that the step index increases in the step-down direction, defined as the positive x direction, as schematically shown in Fig. 2.1.

The adatoms undergo driven diffusion from the electric field. The biased diffusion flux of adatoms with density c takes the form:

$$\mathbf{J}_\alpha = -D_\alpha \nabla c_\alpha + D_\alpha \frac{\mathbf{F}}{k_B T} c_\alpha, \tag{2.1}$$

where $\alpha = (t, s)$ indicates the terrace or step region and D_α is the diffusion constant in the corresponding region, which here is taken to be isotropic for simplicity. We also assume that the effective charge is the same in both regions and ignore the small effects of step motion on the steady state adatom density field, since the direct field-induced adatom drift velocity is generally very much larger than the net

velocity of the steps (driven by free sublimation in real experiments) even at high temperatures.

In many studies of step dynamics, because the separation of their respective time scales, it suffices to solve the diffusion problem with fixed step positions and then balance the fluxes locally at a step to determine its motion. This is often called the *quasi-stationary* approximation, and it will be adopted throughout this paper. Thus the static diffusion problem is simply

$$\nabla \cdot \mathbf{J}_\alpha = 0 \tag{2.2}$$

in each region, along with continuity of c and $\mathbf{J}$ at fixed boundaries between terrace and step regions. The normal velocity of the step region is given by mass conservation locally at an infinitesimal portion of the step region

$$v_n \Delta c = \left[\mathbf{J}_t^- - \mathbf{J}_t^+\right] \cdot \hat{n} - \int_s \partial_\tau \left[\mathbf{J}_s \cdot \hat{\tau}\right]. \tag{2.3}$$

Here $\mathbf{J}_t^\pm$ denote diffusion fluxes in the front and back terraces respectively and Δc is the difference of the areal density of the two phases — the solid phase and the 2D adatom gas phase. For simplicity, we take a simple cubic lattice, so that $\Delta c \approx 1/\Omega = a^{-2}$, where a is the lattice parameter. The last term in Eq. (2.3) represents the contribution from diffusion flux in the step region parallel to the step, where τ denotes the arc length.

2.4 Steady State Solutions

Eqs. (2.1-2.3) define the two-region diffusion model. We first consider the steady state solution corresponding to a 1D uniform step train. In this case, the step normal direction coincides with the x direction on terraces, and thus parallel or tangential diffusion in the step region plays no role here. The steady state concentration profile (denoted by a superscript '0') in a two-region unit is easily obtained by solving

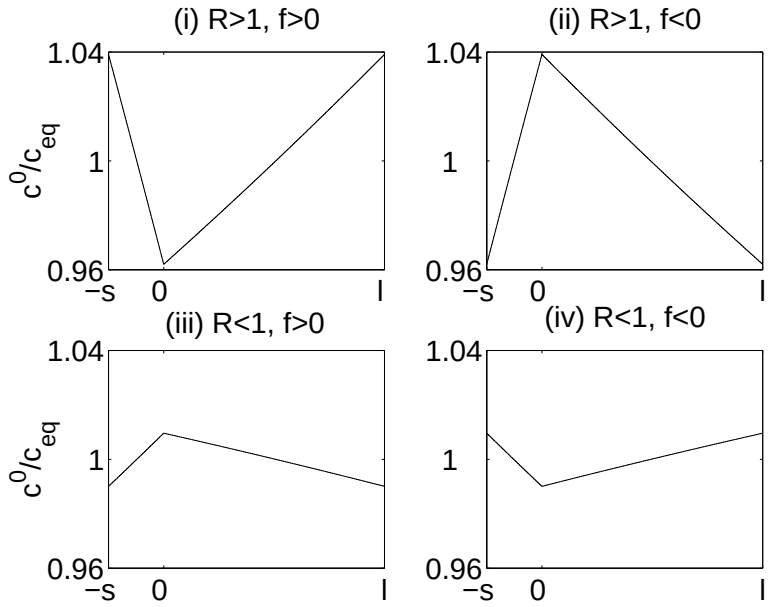

Figure 2.2: Plot of concentration profiles according to Eq.(2.4) with model parameters. $R = 10$ for (i) and (ii), $R = 0.1$ for (iii) and (iv); $|fa| = 0.01$ in all cases.

Eq. (2.2) in both regions subject to continuity of concentration and fluxes at the boundaries and is given by

$$\begin{aligned} c_s^0 &= C\left[R + \frac{(1-R)\left(e^{fl_t}-1\right)}{e^{fl_t}-e^{-fs}}e^{fx}\right] \\ c_t^0 &= C\left[1 - \frac{(1-R)\left(1-e^{-fs}\right)}{e^{fl_t}-e^{-fs}}e^{fx}\right], \end{aligned} \tag{2.4}$$

Here

$$R \equiv D_t/D_s \tag{2.5}$$

is the key dimensionless parameter that describes the relative diffusion rate of adatoms on terraces and in the step regions. $f \equiv \mathbf{F}\cdot\hat{x}/k_BT$ has a dimension of inverse length and characterizes the strength of the external field. l_t is average terrace width in the steady state. C is a constant to be determined shortly.

Evidently, it is the interplay between the external electric field and changes in the local diffusion rates, characterized by various combinations of the two pa-

rameters f and R, that causes the intriguing instabilities. With the electric field perpendicular to the step region, altogether there are four types of steady state adatom concentration profiles with different combinations of parameters f and R, as shown in Fig. 2.2.

In the absence of sublimation, the concentration profiles we obtain here are completely driven by the external field. By taking the limit $f \to 0$ in Eq. (2.4), one should recover the equilibrium concentration (denoted as c_{eq}) on the entire surface. This fixes the constant in Eq. (2.4) as

$$C = c_{eq} \left(l_t + s \right) / \left(l_t + Rs \right). \tag{2.6}$$

Note that the steady state concentration profile of adatoms given by Eq. (2.4) reduces to a constant on the entire surface in presence of the field if the diffusion in the normal step direction is the same as terrace diffusion, i.e., when $R = 1$.

Moreover, the constant flux at the steady state can be written as

$$J_0(l) = D_t c_{eq} f \frac{l}{l + (R-1)s}, \tag{2.7}$$

where

$$l \equiv l_t + s \tag{2.8}$$

is the distance between the centers of two adjacent step regions in a uniform step train. When $R = 1$, a uniform flux $D_t f c_{eq}$ results, independent of terrace widths.

2.5 Step Bunching and Wandering Instabilities

In this section, we study the stability of the steady state solutions. In particular, the physical origins of both step bunching and wandering instabilities are qualitatively discussed.

2.5.1 Step Bunching Instability

A common feature of all steady state profiles shown in Fig. 2.2 is that adatom concentration gradients build up in both terrace and step regions. Under experimentally relevant conditions the field is sufficiently weak that $fs < fl_t \ll 1$ and *linear* concentration (or chemical potential) gradients form. It is then easy to see that the local equilibrium boundary condition $c = c_{eq}$ in the center of the step region holds automatically by symmetry. In the qualitative picture of step bunching discussed by Liu and Weeks [35], a positive terrace concentration gradient (induced in their model by a step-down current with an attachment barrier at a sharp step edge) leads to step bunching. The steady state profile they analyzed leading to step bunching in temperature regime I is very similar to case (i) in Fig. 2.2. This corresponds in the two-region model to a step-down field with slower diffusion in the step region, in agreement with an intuitive picture of a step barrier.

Moreover, it is clear that profile (iv) is qualitatively the same as (i). Hence we expect that the steady state (iv), corresponding to *faster* diffusion in the step region with a *step-up* field, also undergoes a bunching instability. The feature of faster diffusion inside the step region considered here is qualitatively similar to the simulation model studied by Suga *et al.*[42], and indeed they observed a step bunching instability with the step-up current.

To understand the bunching of straight steps it is useful to consider a 1D version of Eq. (2.3):

$$v_n = \Omega \left[J_0 \left(l_{n-1} \right) - J_0 \left(l_n \right) \right], \tag{2.9}$$

where the 1D flux J_0 as given by Eq. (2.7) now depends on the local terrace widths. Consider a small deviation $\delta x_n = \varepsilon_n e^{\omega_1 t}$ for nth step from the steady state, where $\varepsilon_n \equiv \varepsilon e^{in\phi}$ and ϕ is the phase between neighboring steps. Then the step will move as a result of the unbalanced fluxes induced by changing width of the terrace in front $l_n = l + \varepsilon_n \left(e^{i\phi} - 1 \right)$ and back $l_{n-1} = l + \varepsilon_n \left(1 - e^{-i\phi} \right)$. The amplification rate ω_1 is

given by $\omega_1 = v_n/\varepsilon_n$, and substituting into Eq. (2.9) gives

$$\begin{aligned} \omega_1 &= -2\Omega D_s \frac{dJ_0(l)}{dl}(1-\cos\phi) \\ &= 2\Omega D_t c_{eq}^0 \frac{f(R-1)s}{[l+(R-1)s]^2}(1-\cos\phi). \end{aligned} \tag{2.10}$$

Clearly, step bunching occurs when $f(R-1) > 0$, corresponding to two different regimes discussed above, and in both cases the most unstable mode is a step pairing instability with $\phi = \pi$.

2.5.2 Step Wandering Instability

The 1D steady state concentration profiles also provide important insights into step wandering, which is essentially a 2D phenomenon. It is clear that the concentration gradient on the terraces in cases (i) and (iv) can drive a step wandering instability. The monotonically increasing terrace chemical potential tends to make a forward bulging part of a step move even faster, as was first demonstrated for vicinal surfaces by Bales and Zangwill [43, 44]. This is the essence of the classic Mullins-Sekerka instability [45, 46]. However, as shown above, these same profiles lead to 1D step bunching, which tends to suppress the wandering instability. Moreover, this mechanism cannot explain the behavior in regime II of Si(111) where wandering and bunching occur for *different* current directions.

The fact that this step wandering cannot be of the Mullins-Sekerka type driven by terrace gradients suggests that it may originate from mass transport in the *step* region. Let us focus on a single 2D step region, as in Fig. 2.3. In this case, it is convenient to describe the step region using curvilinear coordinates set up by the local normal and tangential directions of the step. For a long wavelength step fluctuation with wavenumber q, there exists a nonzero component of the field in the tangential direction, which induces a driven flux along the step proportional to fq^2. For a step-down field ($f > 0$), this driven flux is destabilizing since it tends to transport mass from "valleys" to forward-bulging "hills". On the other hand, the

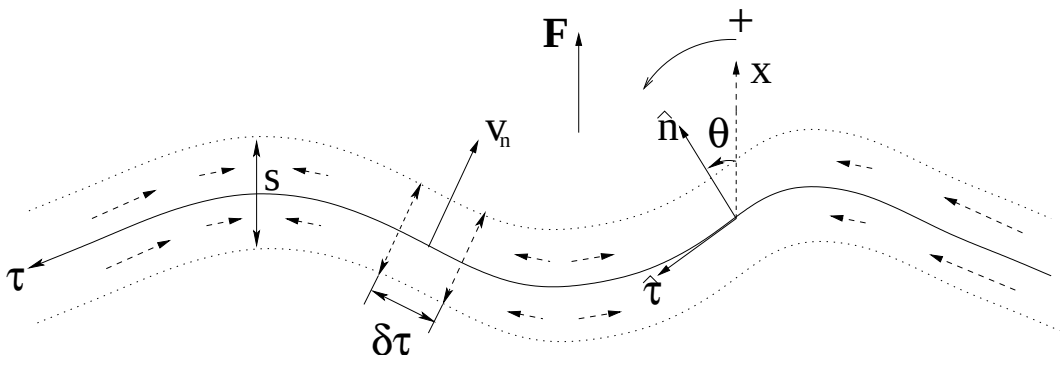

Figure 2.3: A geometrical view of a single wandering step region. $\hat{n}$ and $\hat{\tau}$ denote the normal and tangential direction of the step respectively, and angle θ is between step normal $\hat{n}$ and the average step-down direction along x-axis. The dashed arrows inside the step region schematically shows the driven flux that is parallel to the step for a step-down (x direction) field.

stabilizing flux due to the curvature relaxation is proportional to Γq^4, where Γ is an effective capillary length in the step region. The competition between these two terms results in a finite wavelength linear instability, occurring on a length scale of order ξ, where

$$\xi \equiv \sqrt{\Gamma / |f|}. \tag{2.11}$$

In principle this new wandering instability could arise in cases (i) and (iii) of Fig. 2.2 where there is a step-down field. However step bunching also occurs for case (i). Only case (iii) with $f > 0$ and faster diffusion in the step region ($R < 1$) is free of step bunching, and thus capable of explaining experiments in Regime II of Si(111). In the following sections we show that these qualitative conclusions are in agreement with the quantitative linear stability analysis based on a mapping of the two-region model to the equivalent sharp step model.

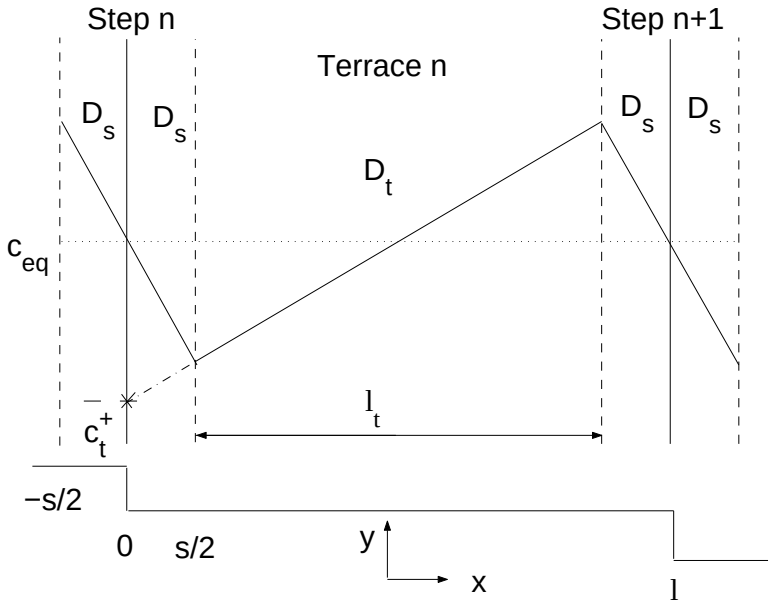

Figure 2.4: Shown is a highly exaggerated profile for a downhill force and slower diffusion in the step region. Also illustrated with the dashed-dot line is the extrapolation of the terrace profile to the center of the step region, thus determining the parameter $\bar{c}_t^+$ in Eq. (2.12). The lower part of the figure gives a side view of sharp equilibrium steps and their associated step regions.

2.6 Mapping to A Generalized BCF Model

In this section we show how the two-region model can be used to generate the appropriate sharp step boundary conditions by a mapping to a generalized BCF model.

The general continuum boundary condition in the sharp-step model assumes small deviations from local equilibrium and introduces linear *kinetic coefficients* $k_\pm$ to relate $\bar{c}_t^+$ (or $\bar{c}_t^-$), the limiting lower (or upper) terrace adatom density at the step edge, to the associated terrace adatom flux into the step. To linear order in the field this gives rise to the standard sharp step boundary condition:

$$\pm D_t \left[\nabla c_t - f c_t\right]_\pm = k \left(c_t - c_{eq}\right)_\pm . \tag{2.12}$$

Here k is the corresponding sharp step kinetic coefficient, which is taken to be symmetric in this case, since there has been evidence for the absence or a very small Ehrlich-Schwoebel effect on Si(111) [47, 48, 49].

A natural way of relating the steady state solutions of the two-region model to those of sharp step model is to *extrapolate* the terrace concentration profile to the center of the step region. This corresponds to a physical coarse-graining where the step region has negligible width when compared to the terrace widths. The use of extrapolation to relate the parameters in discrete and continuum models is well known in other interface applications [50]. We use Eq. (2.4) to evaluate the gradient, and identify $c_t^{\pm}$ as the extrapolated value of terrace concentration at the atomic step, as illustrated in Fig. 2.4. Substituting into Eq. (2.12), to lowest order in the field we find that

$$d \equiv \frac{D_t}{k} = \frac{1}{2}(R-1)s. \tag{2.13}$$

Note that the terrace width l in the sharp step model is naturally related to the two-region width l_t by $l = l_t + s$, as in Eq. (2.8). Here d is often referred to as the attachment-detachment length.

Equation (2.13) gives a mapping of the parameters in the simplest two-region model to those of a generalized BCF model. When $R > 1$ (faster diffusion in the terrace region), k is positive, which leads to a bunching instability for a step-down current. When $R = 1$ (the diffusion rate is the same in both regions), k goes to infinity, which forces $c_t^{\pm}$ in Eq. (2.12) to equal c_{eq}, corresponding to local equilibrium with no instability. When $R < 1$ (diffusion is faster in step regions than in terrace regions), k becomes *negative*, which leads to step bunching by a step-up current together with step wandering by a step-down current.

The possibility of a negative kinetic coefficient, or equivalently a negative d, was first suggested in the work of Politi and Villain [51], though with no derivation or discussion of any physical consequences. Note that even though the derivation given here considers a terrace concentration profile obtained by electromigration,

Eq. (2.13) is a general result that is independent of the field. In Chapter 4 we shall derive general sharp step boundary conditions by considering a discrete hopping model with different hopping rates in two regions but without the field, and there Eq. (2.13) is recovered.

2.7 Linear Stability Results

With the mapping defined by Eq. (2.13), the linear stability analysis can be performed using a standard sharp step model, with parameters obtained from the physically suggestive two-region model. The general calculation is quite cumbersome. Here we omit the algebraic detail and concentrate on the resulting stability in the weak field ($fl \ll 1$) and long wavelength ($ql \ll 1$) limit. The real part of the stability function can be written as

$$\omega_r = \omega_1 (f, \phi) + \omega_2 (q, f, \phi), \tag{2.14}$$

where

$$\omega_1 = \Omega D_t c_{eq}^0 \frac{4df}{(l+2d)^2} (1 - \cos\phi), \tag{2.15}$$

and

$$\begin{aligned} \omega_2 = \Omega D_t c_{eq}^0 q^2 \Bigg\{ & -\Gamma \left[\frac{2(1-\cos\phi)}{l+2d} + \left(l + \frac{s}{R} \right) q^2 \right] \\ & + f \left(\frac{2dl}{l+2d} + \frac{s}{R} \right) \Bigg\}, \end{aligned} \tag{2.16}$$

ω_1 characterizes the 1D instability and thus is independent of q. The bunching instability occurs for $df > 0$ with most unstable mode giving step pairing with $\phi = \pi$. Note that Eq. (2.15) is identical to Eq. (2.10), when Eq. (2.13) is used.

ω_2 characterizes 2D wandering instabilities with respect to perturbations of wavenumber q. The first term on the right hand side is stabilizing, and has its minimum value for $\phi = 0$, where it is proportional to Γq^4 and all the steps wander in phase.

Table 2.1: Linear Stability Results

	$d > 0$ $(R > 1)$	$d < 0$ $(R < 1)$
$f > 0$	Bunching with maximum mode $\phi = \pi$ Wandering with maximum mode $\phi = 0$	Wandering with maximum mode $\phi = 0$
$f < 0$	Linearly stable	Bunching with maximum mode $\phi = \pi$

The second term, proportional to the field, contains two destabilizing contributions. The first contribution, proportional to $D_t df q^2$, describes a Mullins-Sekerka or Bales-Zangwill instability induced by the terrace concentration gradient that can occur when $df > 0$. The second contribution, proportional to $D_s s f q^2$, represents an alternative mechanism for step wandering induced by field-driven periphery diffusion along the step. When $d > 0$, both mechanisms operate with a step-down current, while the step-up case is completely stable. When $d < 0$, the second mechanism can produce wandering with a step-down current, while bunching occurs for a step up current, as was discussed earlier in Sec. (2.5.2). These stability results are summarized in Table 2.1.

2.8 Implications and Comparison with Experiments

Thus far, both step bunching and wandering instabilities have been analyzed in general terms based on the simple idea of two-region diffusion. Now we examine the implications for vicinal Si(111) surfaces. If we assume for concreteness that reconstruction is generally associated with slower adatom diffusion, we can give a qualitatively reasonable scenario that can account for many features of the electromigration experiments observed on Si(111).

In temperature range I, we assume there exists reconstruction in both step

and terrace regions. Consistent with the analysis of Liu and Weeks, we assume that at low temperature the adatom diffusion in the reconstructed step region is slower than in the terrace region, i.e. $R > 1$, corresponding to cases (i) and (ii) in Fig. 2.2. A step-down current induces both step bunching and step wandering of Mullins-Sekerka type. However, the wandering is likely suppressed by the bunching instability. A step-up current produces a stable uniform step train.

At higher temperatures, we expect reconstruction in step region could have a more fragile structure when compared to that in the terrace region since step atoms have more dangling bonds. Thus, there could exist an intermediate temperature range where because of changes in the step reconstruction, diffusion is faster in the step region than on terraces, i.e. $R < 1$, corresponding to cases (iii) and (iv) in Fig. 2.2. The uniform step train now exhibits bunching with a step-up current. Wandering occurs with a step-down current, induced by driven diffusion parallel to the step. In particular, if we substitute in Eq. (2.11) the latest experimental values for the step stiffness [52], $\tilde{\beta} = 16.3 meV/\mathring{A}$, and for the effective charge [38] $z^* = 0.13$, and use a typical electric field strength of $E = 7V/cm$, the resulting wavelength is roughly given by $\lambda \simeq 2\pi\xi \sim 5\mu m$, comparable with experimental values [29, 30, 31] of $6 - 9\mu m$.

In this picture, the transition between different temperature regimes is associated with local equilibrium where $R = 1$. Conceivably, such a transition could happen again at higher temperatures, since only small changes in the relative diffusion rates can take the fundamental parameter R from less than to greater than unity and vice versa. This scenario provides a consistent interpretation of experiments in the second temperature regime and suggests more generally why there could be such a complicated temperature dependence.

2.9 Summary

In this chapter we consider current-induced instabilities on Si(111) surfaces and its seemingly mysterious dependence on temperature. We have studied a physically suggestive two-region diffusion model. The basic idea is to consider different hopping rates associated with different reconstruction and rebonding in the terrace and step regions. The resulting steady state profiles provide important insight into the physical origins of both step bunching and wandering instabilities. Step bunching is induced by positive chemical potential gradients on terraces that are essentially determined by the sign of $f(R-1)$ or equivalently fd in sharp step models. We show that in-phase step wandering observed on Si(111) electromigration does not arise from the well known Mullins-Sekerka instability. Rather, it is induced by driven diffusion along the step edge under the influence of a step-down force, and only becomes significant when step bunching is absent, which requires a negative kinetic coefficient.

We also carried out a mapping from the two-region model to a sharp step model using a simple extrapolation procedure. The result connects the kinetic coefficients in sharp step models to relative diffusion rates in terrace and step regions. In particular, the lowest order result shows that the kinetic coefficients are independent of the driving field, in contrast to earlier suggestions [42].

A coherent scenario for Si(111) electromigration is proposed based on the linear stability analysis of the model. In particular, the mysterious second temperature regime is interpreted using a negative kinetic coefficient. This allows the step wandering that generally occurs with a step-down force to be separated from step bunching. The transition between different temperature regimes is governed by the relative diffusivity in the terrace and step regions. Other theories can predict a reversal of step bunching arising from a change in step transparency [40, 41] or from a change of sign of the effective charge [36]. However, neither approach can give a consistent treatment for step wandering.

Chapter 3

Current-Induced Instabilities on Vicinal Si(001) Surfaces

3.1 Step Bunching on a Si(001) Dimple

In Chapter 2 we have discussed current-induced instabilities on Si(111) surfaces. At similar temperatures vicinal Si(001) surfaces miscut along [110] exhibit step bunching from current normal to the steps in *both* directions [53, 54]. The most notable differences in current-induced step bunching on Si(001) and Si(111) surfaces arise from the (2×1) surface reconstruction (dimerization) on Si(001), which persists up to temperatures of at least $1200°C$ [55]. Two characteristic directions on the surface are established by dimerization, either parallel or perpendicular to the substrate dimer rows in the orthogonal [110] direction, denoted by $\parallel$ and $\perp$ respectively. Experimental evidence suggests that the diffusion along the dimer rows is much faster at low temperatures, i.e., $D_t^{\parallel} \gg D_t^{\perp}$ [56].

In recent experiments [57], the bunching behavior has been studied on dimple geometries, where steps of all orientations are found. As schematically shown in Fig. 3.1a, there are in general two angles needed to describe the local geometry of the dimple when the electric field is applied [57], characterized by the angle θ between

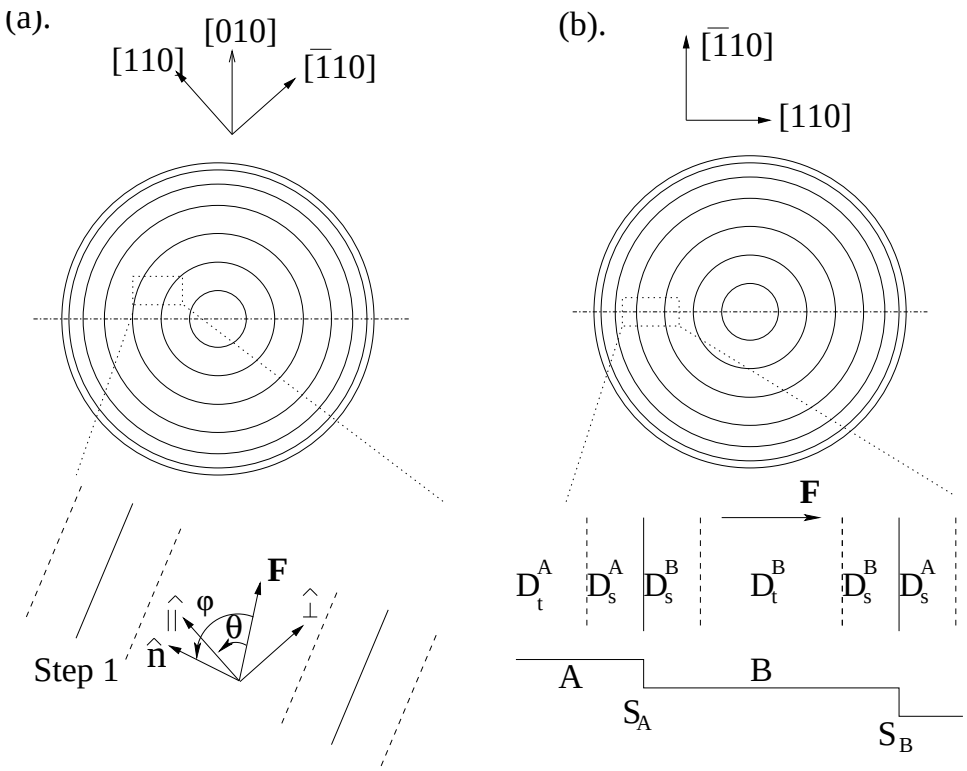

Figure 3.1: A schematic illustration of the dimple geometry on the Si(001) surface. (a) The general view of the dimple with the crystallographic directions indicated above. Zooming into a given local area of the dimple (the dotted line box), we show the step-terrace configuration with a general direction of the electric field. φ is the angle between field direction and the local normal to the steps, while θ is the angle between the field and [110]. $\theta = \pi/4$ corresponds to a field direction along [010]. (b) The top view of the dimple when $\theta = 0$. Zooming into the dotted-lined box near the center of the dimple with $\varphi = 0$, we show a top view of the vicinal surface and a side view of the step-terrace configuration. Most of basic physics of step pairing and bunching will be illustrated in this simple 1D geometry with the electric field perpendicular to average step position.

direction of the electric field and the [110] direction, and the angle φ between the field and the local normal to the steps.

The bunching exhibits interesting angular dependences. When the current is parallel to the orthogonal [110] direction ($\theta = 0$), the bunching is observed to be strongest in the areas where the current is locally parallel to the step normal direction ($\varphi = 0$), e.g., the dotted line box in Fig. 3.1b. No bunching occurs in the corresponding perpendicular directions ($\varphi = \pi/2$). However, if the current is rotated to $\pi/4$ off the dimer row direction ($\theta = \pi/4$), the strongest bunching occurs in the areas where the current is perpendicular to the local step directions ($\varphi = \pi/2$). No bunching is seen in the corresponding perpendicular direction ($\varphi = 0$), which in the previous case was where the maximum bunching was found. In the following discussion, we will first study the instabilities for the simplest case as shown in the dotted line box in Fig. 3.1b ($\theta = 0$ and $\varphi = 0$), and then generalize our results to arbitrary θ and φ.

3.2 Domain Conversion and Step Pairing

Let us begin with the simplest case, where the vicinal surface is misoriented in the [110] direction. At equilibrium rather straight S_A steps that run parallel to the dimer rows of the upper A terrace alternate with much rougher S_B steps that run perpendicular to the dimer rows of the upper B terrace. Here we have used the notation of Ref. [58], where related instabilities during growth are examined. When the field is normal to the steps, as illustrated in the boxed region of Fig. 3.1b, the terrace diffusion rates normal to the steps satisfy $D_t^B \gg D_t^A$.

We assume that the dimerization persists, at least to some extent, on both adjacent half-step regions around each terrace and will similarly affect diffusion rates there. The normal diffusion in the two half-step regions around a given step is characterized by D_s^A and D_s^B. Taking account of the differences in terrace diffusion

rates, it seems reasonable to assume at least that $D_s^B \geq D_s^A$, or

$$\left(D_t^B - D_t^A\right)\left(D_s^B - D_s^A\right) \geq 0. \tag{3.1}$$

Special cases of this assumption include classical local equilibrium steps where $R^A = R^B = 1$ and a symmetric step model where $D_s^B = D_s^A$. The assumption here essentially states that the fundamental physics on Si(001) surfaces is dominated by the alternating reconstruction domains on terraces. Under this assumption, it is natural to think of the surface as made up of alternating A and B units, where the unit α ($\alpha = A$ or B) contains an α terrace together with the two neighboring α half step regions.

We consider here cases where the system is driven away from equilibrium only by the electric field and neglect evaporation. We make the same assumption as for Si(111) that the atomic step always maintains local equilibrium at the temperature of our interest. This assumption effectively eliminates the step transparency (See Chapter 4 for detailed discussion). Thus it decouples the concentration fields on the terraces, and permits a simple solution to the steady state diffusion problem in terms of exponential functions e^{fx} ($f \equiv \mathbf{F} \cdot \hat{x}/k_B T$), as we have seen in the Si(111) steady state.

Assuming the same positive effective charge on the entire surface, the weak field limit ($fs \ll fl_t \ll 1$, where s and l_t are the width of the step and terrace regions as before) allows us to obtain piecewise linear profiles for the adatom concentration. It is straightforward to write down the general solution for the adatom density in unit α as

$$c^\alpha(x) = \begin{cases} c_{eq} + m_s^\alpha \left(x + \frac{l_t^\alpha + s}{2}\right) & -\frac{l_t^\alpha + s}{2} \leq x \leq -\frac{l_t^\alpha}{2} \\ c_{eq} + m_t^\alpha x & -\frac{l_t^\alpha}{2} \leq x \leq \frac{l_t^\alpha}{2} \\ c_{eq} + m_s^\alpha \left(x - \frac{l_t^\alpha + s}{2}\right) & \frac{l_t^\alpha}{2} \leq x \leq \frac{l_t^\alpha + s}{2} \end{cases} \tag{3.2}$$

where l_t^α is the α terrace width. In the above expression the origin is set at the center of the terrace region to take maximum advantage of symmetry. It is easy to transform the origin to the left atomic step position in accordance with the previous

discussion on Si(111) steady state, and the results below will not be altered by any specific choice of the coordinate system.

The $m^{\alpha}_{s,t}$ can be obtained by requiring continuity of concentration and flux at $\pm l^{\alpha}_t/2$ and are given by

$$\begin{aligned} m^{\alpha}_t(l^{\alpha}_t) &= c_{eq} s f \left(R^{\alpha}-1\right) / \left(l^{\alpha}_t + R^{\alpha} s\right) \\ m^{\alpha}_s(l^{\alpha}_t) &= c_{eq} l^{\alpha}_t f \left(1-R^{\alpha}\right) / \left(l^{\alpha}_t + R^{\alpha} s\right) \end{aligned} \tag{3.3}$$

Here $R^{\alpha} \equiv D^{\alpha}_t / D^{\alpha}_s$ gives a dimensionless measure of the relative diffusion rates in the α unit between the terrace and step regions in a direction perpendicular to the step direction, and c_{eq} is the average concentration for a uniform step array when $f = 0$. Again the sign of the concentration gradient on the terrace of the α unit is determined by the product of $f(R^{\alpha}-1)$.

In the quasi-static approximation the step velocities are computed by a flux balance. The surface flux normal to the step is constant throughout the α unit and is exactly given by

$$J^{\alpha}_0 = D^{\alpha}_t c_{eq} f \frac{l^{\alpha}_t + s}{l^{\alpha}_t + R^{\alpha} s}. \tag{3.4}$$

Because of the perfect sink assumption, the fluxes in the individual α units on either side of a step are independent of each other. Thus the step velocity is easy to compute for a given step configuration.

Consider in particular the initial velocity of step S_{α} in a uniform step train ($l^A_t = l^B_t = l_t$). This is given by

$$\begin{aligned} v^{\alpha}_0 &= \Omega \left(J^{\alpha}_0 - J^{\beta}_0 \right) \\ &= \Omega c_{eq} f \left(l_t + s\right) \frac{\left[\left(D^{\alpha}_t - D^{\beta}_t \right) l_t + \left(D^{\alpha}_s - D^{\beta}_s \right) s R^{\alpha} R^{\beta} \right]}{\left(l_t + R^{\alpha} s\right)\left(l_t + R^{\beta} s\right)} \end{aligned} \tag{3.5}$$

where $\alpha, \beta = A$ or B and Ω is the atomic area. In this case the velocities of the two types of steps satisfy $v^B_0 = -v^A_0$. Therefore the initial uniform step array is not a steady state. Depending on the direction of the electric field, one reconstruction

domain expands while the other shrinks, creating step pairs separated by the minor terrace. With a step-down current one finds double height D_B steps (consisting of an upper S_B step and a lower S_A step with a narrow A terrace trapped in between) separated by wide B terraces; the equivalent configuration with D_A steps and narrow B terraces is seen for an step-up current. Experiments show that this field-driven step pairing continues until it is balanced at short distances, probably by step repulsions, as first suggested by Natori *et al.* [59], in the special case where local equilibrium was assumed for all the steps, corresponding to $R^A = R^B = 1$ in our model.

3.3 Mapping of the Effective Step Region

Now let us examine the stability of arrays of such paired steps. Assuming that the step pairs (boundaries of the minor domain) with constant spacings persist throughout the bunching process, as is shown by experiments, we can define a symmetric effective two-region model that can describe the continued bunching of the paired steps. To that end, we treat the minor reconstruction terrace together with the two step regions bounding it as an effective step region that separates one major terrace from another, as schematically shown in Fig. 3.2 for the case of a step-down current. As shown below the bunching behavior is determined by the field direction and the sign of the kinetic coefficient for the sharp step model associated with the effective two-region model defined here.

In Section 2.6 we discuss the mapping to a sharp step model from continuum concentration profiles, assuming local equilibrium atomic step in the middle of the step region. In the present case a minor terrace resides at the center of the effective step region. Nevertheless, we can still follow the extrapolation procedure of concentration profiles in section 2.6, except that we need to take into account of the minor domain in the middle. First we note that the effective equilibrium concentration in

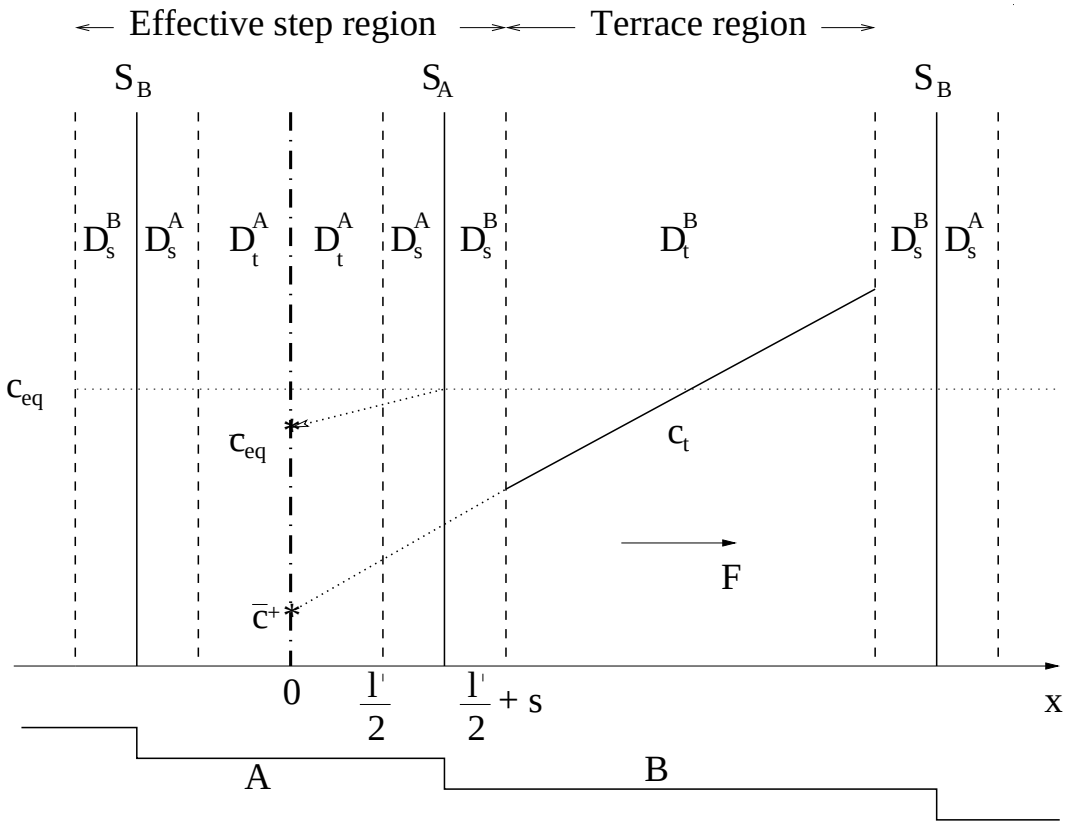

Figure 3.2: A schematic illustration of extrapolation for an effective step region. With a step-down current, domain (1×2) expands to form an effective terrace region with some typical concentration profile c_t. On the other hand, domain (2×1) shrinks to l' and forms an effective step region when combined with the two step regions bounding it. c_t is extrapolated to the dotted-dashed line at $x = 0$ in the middle of the minor terrace which represents the effective "sharp" step.

the center $\bar{c}_{eq}$ is linearly modified by the weak field from its value c_{eq} at the "real" local equilibrium step near the lower boundary of the effective step region, so that

$$\bar{c}_{eq} = c_{eq}\left[1 - \frac{1}{2} f\left(l' + s\right)\right], \tag{3.6}$$

where l' is the width of the minor reconstruction domain.

Next we proceed as before and find that the effective sharp step boundary condition takes a form analogous to Eq. (2.12)

$$D_t^\alpha \left[\nabla c|_+ - f\overline{c}^+\right] = \bar{k}^\alpha \left(\overline{c}^+ - \bar{c}_{eq}\right), \tag{3.7}$$

where D_t^α, $\alpha = A$ or B, is the normal diffusion constant in the major terrace. And the analog of Eq. (2.13) is given by

$$\bar{d}^\alpha \equiv \frac{D_t^\alpha}{\bar{k}^\alpha} = \frac{\bar{s}}{2}\left[\bar{R}^\alpha - 1\right], \tag{3.8}$$

where $\bar{s} = l' + 2s$ is the width of the effective step region and $\bar{R}^\alpha = sR^\alpha/\bar{s}$ is the relative diffusivity in the effective two region model defined above. The concentration extrapolation is schematically depicted in Fig. 3.2 for the case of a step-down current.

Two new features are seen in Eq. (3.7) arising from the use of a single effective step region to describe the paired steps. First, the major terrace is determined by the current direction in the initial step pairing regime. Second, both an effective kinetic coefficient $\bar{k}$ and an effective "equilibrium concentration" $\bar{c}_{eq}$ appear in the sharp step boundary condition.

3.4 Simultaneous Step Bunching in Both Current Directions

Equations (3.7)-(3.8) give the mapping between the effective two region model describing paired steps separated by major terraces and an equivalent sharp step

model. In the steady state where the major terraces all have the same width, the surface flux in the sharp step model can be obtained from Eq. (3.4) as follows. We replace the parameters c_{eq}, s, and R^α by the corresponding effective parameters $\bar{c}_{eq}$, $\bar{s}$, and $\bar{R}^\alpha$. Clearly $l = l_t + \bar{s}$ represents the terrace width in the sharp step model. The steady state flux in the sharp step model as a function of the terrace width is thus given by

$$J_0^\alpha(l) = D_t^\alpha c_{eq} f \frac{l}{l + 2\bar{d}^\alpha}. \tag{3.9}$$

Note that $\alpha = A$ or B is determined by the current direction.

To examine the stability of the above steady state, consider a small deviation $\delta x_n = \varepsilon_n e^{\omega t}$ of the n^{th} step in the uniform step train, where $\varepsilon_n = \varepsilon e^{in\phi}$. Here ε is a small constant and ϕ is the phase between neighboring steps. Then the n^{th} step will move in response to the unbalanced flux induced by the changed widths of the terraces in front $l_n = l + \varepsilon_n(e^{i\phi} - 1)$ and back $l_{n-1} = l + \varepsilon_n(1 - e^{-i\phi})$. The linear amplification rate $\omega = v_n/\varepsilon_n$ is given by

$$\omega = \Omega D_t^\alpha c_{eq} \frac{4\bar{d}^\alpha f}{\left(l + 2\bar{d}^\alpha\right)^2} \left(1 - \cos\phi\right). \tag{3.10}$$

An instability towards step bunching results if $\bar{d}^\alpha f > 0$ with a maximum at $\phi = \pi$, corresponding to step pairing. Note that the direction of the field and the sign of the effective kinetic coefficient combine to determine when step bunching occurs, the same as Si(111) discussed earlier.

Using Eqs. (3.8) and (3.10), we see that to get simultaneous step bunching from current in *both* directions seen in experiments, the following inequality has to hold

$$R^A > 2 + \frac{l'}{s} > R^B. \tag{3.11}$$

With a step-down current, the first part of the inequality in Eq. (3.11) makes the effective kinetic coefficient for the effective step region containing the slower diffusion domain positive, which results in a step bunching instability. The second inequality in Eq. (3.11) give rise to a *negative* effective kinetic coefficient which produces step

bunching with a step-up current. Note that this does not require negative kinetic coefficients for single steps of either kind.

However, if one assumes the individual steps are at local equilibrium, ($R^A = R^B = 1$), then the kinetic coefficient for the effective step region is negative in both cases, and therefore bunching is expected only from a step-up current.

3.5 Angular Dependent Step Bunching

It is straightforward to extend the above analysis to a general dimple geometry shown in Fig. 3.1a, where the domain conversion exhibits interesting angular dependences. Again, we need to consider the fluxes from the neighboring terraces going into the step. Using Eq. (3.4), we can represent the surface flux as the sum of fluxes along the two characteristic directions,

$$\mathbf{J}_f = \cos\theta J_0^B \widehat{\parallel} + \sin\theta J_0^A \widehat{\perp} \tag{3.12}$$

for the front terrace and

$$\mathbf{J}_b = \cos\theta J_0^A \widehat{\perp} + \sin\theta J_0^B \widehat{\parallel} \tag{3.13}$$

for the back terrace of step 1 in Fig. 3.1a, where $\parallel$ and $\perp$ are the directions parallel and perpendicular to dimer rows as defined earlier. The angular dependent step velocity is readily obtained

$$v_0^{(1)}(\theta, \varphi) = v_0^B \cos(2\theta - \varphi), \tag{3.14}$$

where v_0^B is given by Eq. (3.5). Eq. (3.14) shows that a steady state of paired steps will form on the part of the dimple where $\cos(2\theta - \varphi) \neq 0$.

In the following, we will concentrate on two special configurations that are studied experimentally [57]. The first is shown in Fig. 3.1b, where the current is parallel to the dimer row direction. In this case $\theta = 0$, and $\cos\varphi$ characterizes the

angular dependence around the dimple. The maximum pairing instability occurs at $\varphi = 0$ where the current is perpendicular to the step normal direction, and no instability in seen at $\varphi = \pm\pi/2$. From the previous discussion in Section 3.2 and Section 3.4, we can easily see that continued step bunching occurs with a maximum at $\varphi = 0$.

The other interesting configuration corresponds to an upright field parallel to [010] direction in Fig. 3.1a. In this case the current is at an angle $\theta = \pi/4$ from the dimer row direction. Hence the angular dependence becomes $\cos(\pi/2 - \varphi) = \sin\varphi$. The maximum pairing instability occurs at $\varphi = \pi/2$, where the current is *parallel* to the steps, and no instability occurs when the current is perpendicular to the steps. Again the sharp step model corresponding to the steady state can be extracted. The subsequent step bunching instability for a parallel current was discussed by Liu *et al.* [60]. Their stability analysis suggests that step bunching generally occurs for a non-vanishing attachment/detachment length d, regardless of its sign, when the current is parallel to the average step positions.

The results discussed here are in good agreement with experiments. For the angular dependent step pairing, the result is consistent with the original analysis by Nielsen *et al.* [57]. However, our explanation for the subsequent step bunching is different. Our analysis provides a simpler scenario that does not require a tensor character to the effective charge.

3.6 Unified View of Current-Induced Instabilities

In this Chapter we analyze current-induced instabilities on Si(001) surfaces along the same lines as is done for Si(111) surfaces. The notable complication arise from the well-known fact that Si(001) has two reconstruction domains. The basic physical

idea here is that the fundamental physics of mass transport on Si(001) surfaces is dominated by the two alternating terrace domains. Hence the two half-step domains have similar diffusion property to the specific terrace domain bounded in between. Together with the local equilibrium assumption at the atomic steps, a simple and coherent account for most of the interesting findings in Si(001) electromigration experiments is obtained. Despite of the seemingly different appearance, the current-induced instabilities on Si(111) and Si(001) surfaces can be interpreted in a simple and unified way.

First of all, the step bunching instability always occurs when the sign of the product fd is positive. For single-domained Si(111) surfaces, the unstable current direction reverses as temperature rises if the sign of d changes, which can give rise to multiple temperature ranges in Si(111). For double-domained Si(001) surfaces at a given temperature, fd can hold the same sign even with a change of current-direction, since the change in current direction leads to different domain conversion and subsequently different sign of d. Hence Si(001) have step bunching simultaneously in both current directions. In fact, based on the discussion in Section 3.4, one can easily map the step-down bunching on Si(001) to Si(111) in temperature range I, and the step-up bunching to Si(111) in temperature range II.

Second, the step wandering instability of Mullins-Sekerka type is also determined by the sign of fd, thus always coincides with the bunching instability. Only when the step bunching is effectively suppressed, step wandering can be observed in the same current direction that normally induces step bunching. One numerical example is given by Sato *at. al.* [61], where step wandering is seen with a step down current for attachment/detachment limited kinetics without transparency (normal condition for step bunching), when an unphysically high step-step repulsion is applied in the simulation. There are also some experimental evidence of some step wandering occurred in the bunching regime, e.g. in Si(001) step-up bunching regime (see figure 4 in Ref. [57]). However, it is clear that to account for the wandering

instability on Si(111) in temperature range II, we need to break the symmetry of fd. As discussed in Chapter 2, the new mechanism we proposed involves the driven diffusion inside the step region, not the terraces. Thus it only depends on the sign of f. When the negative sign of d reverses the bunching current to the step-up direction, the wandering instability stays with the step-down current.

Chapter 4

From Discrete Hopping to Continuum Boundary Conditions

4.1 Kinetic Boundary Conditions and Surface Morphology

Vicinal surfaces which exhibit a uniform train of steps, created by a miscut along a low index plane below the roughening temperature, have long been of great interest in both basic and applied research [62]. High quality crystals can be grown through step-flow — the uniform motion of more or less equally-spaced steps. Moreover, step bunching and wandering instabilities obtained under external driving can create two dimensional patterns that could serve as templates for nanoscale structures and devices. Therefore, the fundamental understanding of the dynamics of the preexisting steps plays a central role in many studies of non equilibrium processes on vicinal surfaces.

Most fundamental studies of the static and dynamic properties of vicinal surfaces are based on generalizations of the classic theory of Burton, Cabrera, and Frank (BCF) [32] that we briefly mentioned in Chapter 2. This theory describes

the diffusion of adatoms on terraces with boundary conditions at steps, which are treated as sharp line boundaries. Originally BCF assumed that the steps acted as perfect sinks and sources of adatoms so that the limiting adatom concentration at the step boundaries always reduces to local equilibrium.

Many extensions and modifications of the BCF theory have been suggested to provide a more general framework for the description of different experiments. One of the most important was Chernov's introduction of linear *kinetic coefficients* [63, 64], which permit deviations from local equilibrium at steps. It was soon recognized that in general the kinetic coefficients could be asymmetric [65, 66]. Another generalization permits step *permeability* or *transparency*, with a term in the boundary condition directly connecting the limiting adatom concentration on adjacent terraces [67]. These generalized BCF models provide a mesoscopic or coarse-grained description of surface evolution with effective boundary conditions at sharp steps, and we will generally refer to them as sharp step models.

Many kinetic instabilities seen in experiments have been successfully described from this perspective using various combinations of boundary conditions. However in general it is not clear how to connect the choices and values of the effective parameters in sharp step models to the underlying physical processes or how to determine the uniqueness of such a mapping. A similar difficulty arises in trying to relate "microscopic" parameters in kinetic Monte Carlo simulations of discrete hopping models to the effective parameters in a generalized sharp step model. Very different microscopic models can sometimes seem to give equally plausible mesoscopic descriptions of limited sets of experimental data.

In Chapter 2 and 3 we proposed a novel continuum two-region diffusion model, which gave a rather simple and unified description of a variety of current-induced instabilities seen experimentally on vicinal Si surfaces. The model assumes that diffusion rates in a finite region around a step could be affected by the different local bonding configurations and thus differ from those found elsewhere on terraces. By

extrapolating the steady state concentration profile to the center of the step region, we obtained a mapping of the parameters in the continuum two region diffusion model to those of an equivalent classical sharp step model. One surprising conclusion was that *negative* kinetic coefficient can arise when the diffusion rate near a step is faster than that on the terraces.

In this chapter, we will provide a more systematic way of deriving the boundary conditions for the continuum sharp step models from a rather general 1D discrete hopping model that permits both asymmetric diffusion in the step region as well as step permeability. As discussed by Ghez and Iyer [68], such an effective 1D model can result from averaging over relevant 2D configurations of kink and ledge sites on an atomic step. This model provides a physical way of connecting microscopic hopping parameters that are used in simulations with the effective parameters in sharp step boundary conditions.

4.2 A 1D Hopping Model Based on Two-region Diffusion

The simple 1D model that we study is schematically shown in Fig. 4.1, where an atomic step site is surrounded by a region of width s with generally different diffusion rates, induced by reconstruction or rearrangements of local dangling bonds. As we will see, this difference can generate effective kinetic coefficients in a sharp step description.

In general, the width s of the step region with different diffusion barriers should vary for different systems. However, it is found that the essential physics of the hopping model is not strongly affected by specific choices of s that is on the order of a few lattice spacings a. Thus we analyze the algebraically simplest case shown in Fig. 4.1 with half-step regions of width a. The more general result in terms of s,

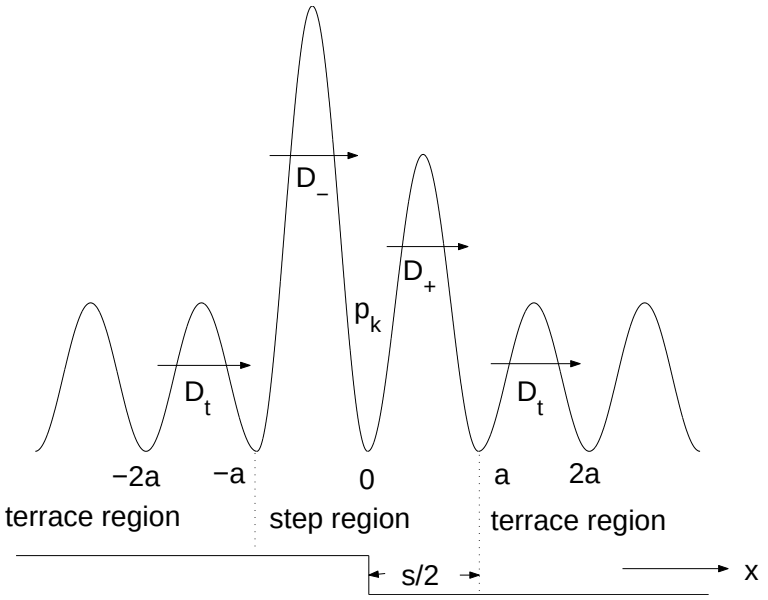

Figure 4.1: A schematic plot of the 1D potential surface near an atomic step. Different D's that have dimensions of diffusion constants characterize the hopping rates associated with different barrier heights. Here, we take the width of the step region to be $2a$.

needed in accordance with the analysis of Si electromigration experiments, is easily obtained by replacing a with $s/2$, as will become clear later when the results of this generic hopping model are compared to our previous results in Chapter 2 and 3.

We include here two additional physical features of the step region as illustrated in Fig. 4.1. One is the possible *asymmetry* in the diffusion processes in the up and down half-step regions, described by hopping rates $D_\pm/a$. The $D_\pm$ have dimensions of a diffusion constant, and the model is usefully characterized by dimensionless parameters

$$R_\pm \equiv D_t/D_\pm, \tag{4.1}$$

with D_t the diffusion constant on the terraces. Here Eq. (4.1) is a natural extension of Eq. (2.5) when the step kinetics is asymmetric.

The other feature we build in is *step permeability* or *transparency*, characterized

in our model by a single parameter p_k ($0 \leq p_k \leq 1$). This can be understood as the effective probability in our 1D model, that an adatom hopping to site 0 will encounter a kink site at a given temperature and thus equilibrate with the solid. This parameter takes account of effects from both kink site density and ledge diffusion in a full 2D model.

When $p_k = 1$, the step site acts as a perfect sink maintained by either enough kink sites or fast ledge diffusion or both, and consequently the step site concentration will be pinned at equilibrium c_{eq}. In the opposite limit with $p_k = 0$ no adatoms are incorporated into the solid. The step site behaves like any other terrace site and thus is perfectly permeable. We neglect other possible sources of permeability, including direct hopping over the step region from one terrace to another or effects of rapid step motion [69], which we believe are less physically relevant for our cases of interest.

In the rest of this chapter, general diffusion fluxes resulting from concentration gradients are considered first, followed by the case of driven diffusion from an external field in the limit $p_k \to 1$, directly corresponding to the examples of electromigration on Si surfaces encountered in Chapter 2 and 3.

4.3 Discrete Diffusion Fluxes

Without the external driving, we assume that the net flux of adatoms that hop between step site 0 and site a can be partitioned into two effective contributions:

$$J_{a/2} = \frac{D_+}{a} \left[p_k \{ c_{eq} - \hat{c}\,(a) \} + (1 - p_k) \{ \hat{c}\,(0) - \hat{c}\,(a) \} \right]. \tag{4.2}$$

The first term describes an adatom exchange with probability p_k involving equilibrated "kink-like" adatoms at site 0 with density c_{eq} and the neighboring terrace site. The second term involves a similar exchange with probability $(1 - p_k)$ involving unincorporated "ledge-like" adatoms with density $\hat{c}\,(0)$. Only the former involves creation/annihilation of adatoms, and the latter is treated as a normal diffusion flux that conserves the adatom density.

Similarly, the flux from site $-a$ to 0 is

$$J_{-a/2} = \frac{D_-}{a}\left[p_k\{\hat{c}\,(-a) - c_{eq}\} + (1-p_k)\,\{\hat{c}\,(-a) - \hat{c}\,(0)\}\right]. \tag{4.3}$$

Since we assume that all the sinks/sources reside only at site 0, the net flux of adatoms that hop from site a $(-2a)$ to site $2a$ $(-a)$ takes on the simpler form

$$J_{\pm 3a/2} = \pm\frac{D_t}{a}\left[\hat{c}\,(\pm a) - \hat{c}\,(\pm 2a)\right]. \tag{4.4}$$

As has been introduced in Section 2.3, we will use the *quasi-static* approximation to simplify the analysis. Here we assume that the motion of the step region is much slower than the relaxation of the terrace diffusion field, so that one can determine the diffusion process on terrace sites with fixed positions of the step regions. In the quasi-static limit the net change in the number of adatoms at each terrace site given by a total flux balance must vanish, i.e., $d\hat{c}(x)/dt = 0$ for $x = \pm a, \pm 2a \ldots$ In particular, at sites $\pm a$, the balance of fluxes is given by

$$0 = \frac{d\hat{c}\,(\pm a)}{dt} = \pm\left[aJ_{\pm a/2} - aJ_{\pm 3a/2}\right]. \tag{4.5}$$

At step site 0, $\hat{c}\,(0)$ can be determined by balancing the conserved flux terms proportional to $(1-p_k)$ in Eqs. (4.2) and (4.3), and is given by

$$\hat{c}\,(0) = \frac{D_+\hat{c}\,(a) + D_-\hat{c}\,(-a)}{D_+ + D_-}. \tag{4.6}$$

4.4 Relating Parameters in Discrete and Continuum Models

Our task now is to relate the physically suggestive parameters $R_\pm$ and p_k in the discrete hopping model to the kinetic coefficients $k_\pm$ and permeability rate P appearing in the boundary conditions of a continuum sharp step model as in Eq. (4.7) below. For $x > 0$, consider a smooth continuum concentration profile $c\,(x)$ that

passes through the discrete concentrations $\hat{c}\,(a)$ and $\hat{c}\,(2a)$. (The caret distinguishes discrete from continuum functions.) The behavior of $c\,(x)$ at larger x is determined by the physical processes on the terraces, but does not need to be specified explicitly for our purposes here.

To make contact with the sharp step model, we rewrite the fluxes in Eqs. (4.2)-(4.5) in terms of $c(x)$. To that end we use a Taylor series expansion to linear order to express $c\,(a) = \hat{c}\,(a)$ and $c\,(2a) = \hat{c}\,(2a)$ in terms of $c^+ \equiv c(0^+)$, the extrapolated limiting concentration as $x \to 0^+$ at the sharp step edge in a continuum picture, and its associated gradient $\nabla c\,|_+$. Similarly, $\hat{c}\,(-a)$ and $\hat{c}\,(-2a)$ can be expressed in terms of c^- and $\nabla c\,|_-$, which in general are different than c^+ and $\nabla c\,|_+$.

Using Eq. (4.6) to eliminate $\hat{c}\,(0)$, and substituting into Eq. (4.5), we find that the result can be rewritten in the form of a generalized *linear kinetics boundary condition* with permeability

$$\pm \left[D_t \nabla c\,|_\pm \mp v c^\pm \right] = k_\pm \left(c^\pm - c_{eq} \right) + P \left(c^\pm - c^\mp \right). \tag{4.7}$$

The kinetic coefficients $k_\pm$ are given by

$$k_\pm = \frac{D_t}{a} \frac{p_k}{(R_\pm - 1)\left[1 + (1 - p_k)\, M\right]}, \tag{4.8}$$

where

$$M \equiv \frac{R_+ R_-}{(R_+ + R_-)} \left[\frac{R_+}{R_- - 1} + \frac{R_-}{R_+ - 1} \right] \tag{4.9}$$

is symmetric on exchange of $+$ and $-$. Note in general that the ratio of the kinetic coefficients satisfies

$$\frac{k_+}{k_-} = \frac{R_- - 1}{R_+ - 1} \tag{4.10}$$

independent of p_k. The permeability rate P can be written as

$$P = \frac{k_\pm}{p_k (R_\mp - 1)} \cdot \frac{(1 - p_k)\, R_+ R_-}{(R_+ + R_-)}. \tag{4.11}$$

Using Eq. (4.8) in the first factor, we see that P is *symmetric* on exchange of $+$ and $-$, and has a finite limit as $p_k \to 0$.

The final parameter v in Eq. (4.7) is zero in our present treatment since we used the quasi-static approximation to derive Eqs. (4.5) and (4.6). In principle, a non-vanishing v would arise if we took the flux due to step motion into account in the discrete hopping model. However, the quasi-static limit is valid in most physical cases of interest, and thus this additional complication can be avoided.

Equations (4.7-4.11) are the central results in this section. As mentioned earlier, we find that the sharp step boundary condition can indeed be generally expressed using linear kinetics with permeability. More importantly, we are able to relate the effective parameters in the sharp step boundary conditions to the physically suggestive parameters we considered in our generic hopping model. This mapping provides a simple way to understand many aspects of kinetic boundary conditions in sharp step models.

4.5 Interpretation of Sharp Step Boundary Conditions

A notable general feature of the results derived in the previous section is that the kinetic coefficients $k_{\pm}$ are proportional to p_k and the permeability rate P is proportional to $(1 - p_k)$. The kinetic coefficients characterize adatom exchange involving equilibrated solid adatoms at kinks and the adatom gas phase, while the permeability rate characterizes adatom motion across the step without equilibrating with the solid phase. Moreover, the kinetic coefficients $k_{\pm}$ are in general asymmetric on the two sides of the step due to the asymmetry of emission and diffusion processes from kinks. However, the permeability rate P is symmetric since the physical processes of hopping from one side to the other without attachment at the step always involves the diffusion constants on both sides.

We now consider some limits of those general expressions to illustrate some

interesting features of both the kinetic coefficients and the permeability rate.

4.5.1 Impermeable steps, $p_k \to 1$

This limit is usually considered in treatments of the sharp step model, and we used it to analyze current-induced instabilities on Si surfaces in Chapter 2 and 3. In this limit the only way for the adatoms to go across a step is through attachment/detachment at kinks, and the permeability rate P vanishes.

The results are conveniently described in terms of the *asymmetric* attachment/detachment lengths

$$d_\pm \equiv D_t/k_\pm. \tag{4.12}$$

Using Eq. (4.8), these are given by

$$d_\pm = a\,(R_\pm - 1)\,. \tag{4.13}$$

If we restrict ourselves in a symmetric case and replace the width $2a$ of the step region in the present model by a general value s, we recover exactly the result of Eq. (2.13) that we found earlier by extrapolating concentration profiles obtained using continuum two region diffusion model. The consistency between the two equations clearly shows the general validity of the mapping between model parameters in previous chapters when diffusion driven by a weak electric field is considered. In fact, as will be shown in Section 4.6 when the external driving field is explicitly taken into account, the above result still holds at least to the lowest order of the field.

For $R_\pm > 1$, corresponding to slower diffusion in the step region, the attachment/detachment lengths and kinetic coefficients are positive. The kinetics is usually called *attachment/detachment limited* when $d_\pm \gg l$, with l the average terrace width in a uniform step train, or *diffusion limited* when $0 \leq d_\pm \ll l$. For $R_\pm = 1$, $d_\pm$ vanishes, and the kinetic coefficients diverge. This forces $c^\pm$ to equal

c_{eq} in Eq. (4.7) and generates the local equilibrium boundary condition originally proposed in the BCF model.

More interestingly, for $R_{\pm} < 1$, corresponding to faster diffusion in the step region, the attachment/detachment lengths and the corresponding kinetic coefficients are *negative*. As we showed earlier, the sign of the kinetic coefficients plays a key role in interpreting electromigration experiments on Si surfaces, since it determines the stability of a uniform step train for a given current direction.

In the following, we will characterize the limit $p_k \to 1$ as defining a *perfect sink* model, since adatoms can not diffuse across a step without attachment/detachment at kink sites. As a direct consequence, the two sides of the step are decoupled and any change of the microscopic rates on one side of the step does not affect the kinetic coefficient on the other side. However, as shown above, the two sides of the step will in general be coupled for $p_k < 1$ through Eqs. (4.10) and (4.11), and the subsequent analysis of step dynamics becomes much more involved.

4.5.2 Very permeable steps, $p_k \to 0$

This limit may be physically relevant at low enough temperatures, or slow enough ledge diffusion, or some proper combination of both. Here the adatoms hop around on the surface without encountering sinks/sources in the step region. Thus one expects vanishing kinetic coefficients, but a finite permeability rate, and this is indeed what Eq. (4.8) and Eq. (4.11) predict in this limit.

As in Eq. (4.12), let us define a corresponding *permeability length*

$$d_P \equiv D_t/P. \tag{4.14}$$

Then Eqs. (4.11) and (4.8) yield

$$d_P = 2a\left[\frac{1}{2}\left(R_+ + R_-\right) - 1\right]. \tag{4.15}$$

Similar to $d_{\pm}$, the permeability length d_P can become *negative* when $(R_+ + R_-) < 2$, with faster diffusion in the step region. Eq. (4.15) is consistent with results derived

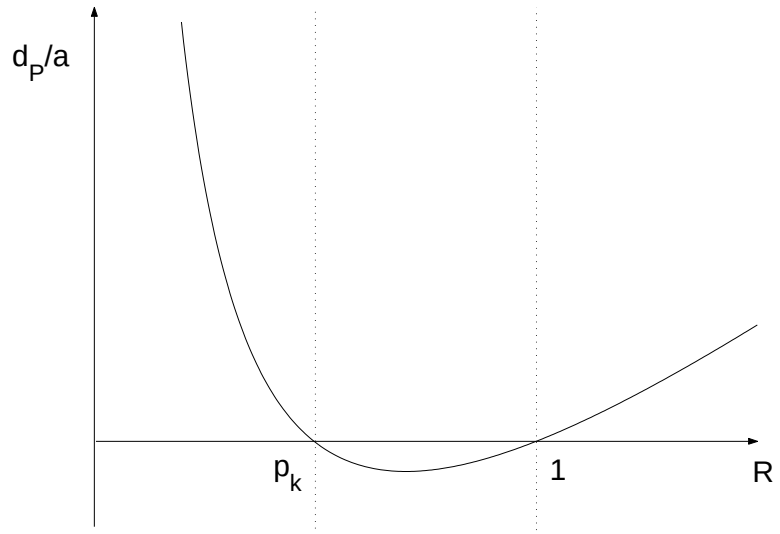

Figure 4.2: Plot of the dimensionless permeability length d_P/a as a function of R in the symmetric case for a general p_k.

from a continuum phase field model [69]. Recently Pierre-Louis and Métois have argued that negative permeability lengths can explain some novel growth-induced instabilities seen during electromigration on Si(111) surfaces.

4.5.3 Partially permeable steps, $0 < p_k < 1$

This is the most general case, where only a finite fraction of adatoms at the step equilibrate at kinks, presumably corresponding to intermediate temperatures with moderate ledge diffusion. We focus on the simplest *symmetric case* where $D_\pm = D_s$ or $R_+ = R_- = R$ in Eqs. (4.8)-(4.11). The attachment/detachment length becomes

$$d = \frac{a}{p_k}\left(R - p_k\right), \tag{4.16}$$

and the permeability length is

$$d_P = 2a\left(R-1\right)\frac{\left(R-p_k\right)}{\left(1-p_k\right)R}. \tag{4.17}$$

Equation (4.16) can be understood using the same physics as in the perfect

sink model. With a finite probability p_k to encounter a kink, an adatom has to move faster in the step region ($D_s = D_t/p_k$) to maintain local equilibrium ($d \to 0$ or $k \to \infty$) compared with the perfect sink case ($D_t = D_s$). The permeability length in Eq. (4.17) is a new feature arising from the possibility that the adatoms go directly across the step without equilibrating with the solid. This expression shows a fairly complicated dependence on microscopic motions characterized by R and p_k.

A schematic plot of d_P versus R for a given p_k is shown in Fig. 4.2. Both d and d_P diverge as $R \to \infty$, since all motion in the step region vanishes in this limit. d_P decreases as R decreases, and stays positive for $R > 1$. Just like the attachment/detachment length, the permeability length changes sign from positive to negative as R passes through 1, with equal hopping rates in the terrace and step regions. However, the permeability length becomes positive again for small enough R when the motion in the step region is sufficiently fast ($R < p_k$) that the probability of crossing the step without involvement of a kink is effectively decreased to a point that it is no longer faster than hopping on terraces.

4.6 A Perfect Sink Model with a Constant Electric Field

In the generic hopping model discussed earlier, we assumed that the flux arose only from concentration gradients. We consider here the case where there is a additional external driving force from the electric field, and take the perfect sink limit $p_k = 1$. In particular, we examine whether or not the kinetic rate parameters in the resulting sharp step model could depend on the field as Suga *et al.* previously suggested [42].

In the absence of the field, the 1D potential energy surface is similar to that in Fig. 4.3, where now the site at $x = 0$ is a perfect sink surrounded by a more general region of width s with different diffusion barriers. When a weak electric field

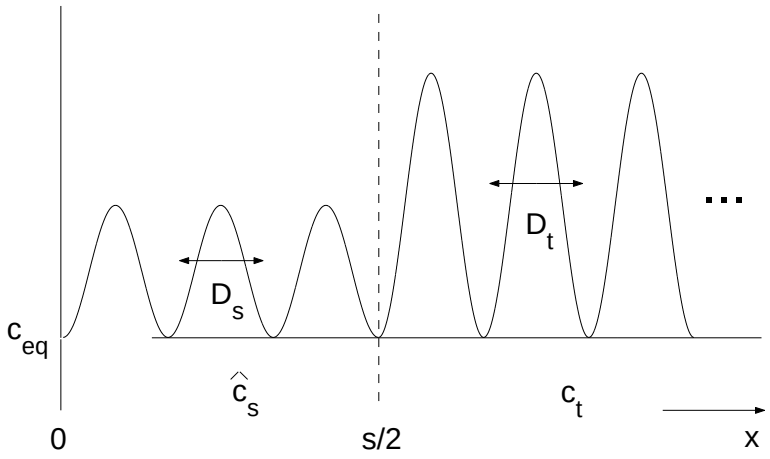

Figure 4.3: A schematic plot of the 1D potential surface for DTR in which a half step region with its neighboring terrace is considered.

is applied in the positive x direction, the potential energy surface will be modified by an amount $V = -\int \mathbf{F} d\mathbf{x}$, where $\mathbf{F} = z^* e\mathbf{E}$, $z^* e$ is the effective charge. The modification of the potential surface produces a bias for adatom hopping, which will later lead to a convective flux contribution in the continuum description.

The driven flux inside the step region can be written as

$$J_{x+a/2} = \frac{D_s}{a} e^{fa/2} \hat{c}_s(x) - \frac{D_s}{a} e^{-fa/2} \hat{c}_s(x+a), \tag{4.18}$$

where $f \equiv |\mathbf{F}| / k_B T$. The quasi-static approximation suggests continuity of fluxes, i.e. $J_{x+a/2} = J_{x-a/2}$, which leads to the following equation for the discrete concentration $\hat{c}_s(x)$,

$$0 = e^{-fa/2} \hat{c}_s(x+a) - \left(e^{fa/2} + e^{-fa/2}\right) \hat{c}_s(x) + e^{fa/2} \hat{c}_s(x-a), \tag{4.19}$$

where x is evaluated at discrete lattice sites inside the step region. It is easy to write down the solution of Eq. (4.19) as

$$\hat{c}_s(x) = c_{eq} + A\left(e^{fx} - 1\right), \tag{4.20}$$

taking account of the perfect sink at $x = 0$. Here A is a constant that can be determined by continuity of fluxes at the boundary between step and terrace region,

i.e. $J_{s/2-a/2} = J_{s/2+a/2}$. This gives

$$A = \frac{e^{-fa/2} R\hat{c}_t \left(\frac{s}{2} + a\right) - \left[e^{-fa/2} + e^{fa/2}\left(R-1\right)\right] c_{eq}}{e^{fa/2}\left(e^{fs/2}-1\right) R + e^{fa/2} - e^{-fa/2}}. \tag{4.21}$$

Here $\hat{c}_t$ is the discrete concentration on the terrace site.

To obtain the sharp interface boundary condition, we apply flux continuity $J_{s/2+a/2} = J_{s/2+3a/2}$, and express all the discrete terrace concentrations in terms of the extrapolated c^+ and the corresponding gradient $\nabla c\,|_+$. In the weak field limit that is valid in most experiments, we can linearize the exponentials in all of the above expressions. To the leading order, we obtain the boundary condition as

$$\pm D_t \left[\nabla c\,|_\pm \mp f c^\pm\right] = k_\pm \left(c^\pm - c_{eq}\right). \tag{4.22}$$

where results for both the + and − sides can be given by symmetry. Note that the term proportional to f is the convective flux induced by the field, which is of the same order as the concentration gradient. As mentioned earlier in Section 4.4, the mapping to the kinetic coefficient is independent of the field to lowest order, and is given by

$$d_\pm \equiv \frac{D_t}{k_\pm} = \frac{1}{2}\left(R_\pm - 1\right) s, \tag{4.23}$$

where $R_\pm \equiv D_t/D_s$. Equation (4.23) recovers the results we derived earlier from continuum two region diffusion model, and is also consistent with the general result in Eq. (4.13).

In the above we discuss the mapping to a sharp step model from a perfect sink model in which the effects of the electric field are treated explicitly, while assuming the perfect sink resides at $x = 0$ - the center of the step region. Now let us turn to examine the effective step region formed as the result of the initial pairing instability on Si(001) electromigration.

In this case a minor terrace resides at the center of the effective step region. We can still follow the treatment above if we take this into account by shifting the origin of the coordinate system by transforming $x \to x - \left(l' + s\right)/2$ and $s/2 \to l'/2 + s$,

where l' is the width of the minor reconstruction domain, see Fig. 3.2 for relevant lengths. Representing the discrete terrace concentrations by a continuum function $c(x)$ and Taylor expanding as before about $x = 0^+$ — the center of the effective step region — we find that the effective sharp interface boundary condition, keeping the same notation as in Section 3.3, takes exactly the same as Eq. (3.7):

$$D_t^\alpha \left[\nabla c|_+ - f\overline{c}^+\right] = \bar{k}^\alpha \left(\overline{c}^+ - \bar{c}_{eq}\right). \tag{4.24}$$

in which the two effective parameters $\bar{c}_{eq}$ and $\bar{k}$ are naturally emerging from the analysis, given by

$$\bar{c}_{eq} = c_{eq}\left[1 - \frac{1}{2}f\left(l' + s\right)\right], \tag{4.25}$$

and

$$\bar{d}^\alpha \equiv \frac{D_t^\alpha}{\bar{k}^\alpha} = \frac{\bar{s}}{2}\left[\bar{R}^\alpha - 1\right], \tag{4.26}$$

where $\bar{s} = l' + 2s$ and $\bar{R}^\alpha = sR^\alpha/\bar{s}$. Eqs. (4.24-4.26) recover the exact results obtained in Section 3.3 without knowing any detailed concentration profiles on terraces.

4.7 Summary

This chapter derives expressions for sharp step boundary conditions characterized by linear kinetics rate parameters $k_\pm$ and P for general BCF type models by appropriate coarse-graining from a microscopic hopping model. $k_\pm$ and P are related to the attachment/detachment kinetics at kinks and to diffusion across the ledges respectively. In particular, the study shows that both parameters can be negative when diffusion is faster in the step region than on terraces. The possibility of negative kinetic coefficients was first suggested by Politi and Villain [51], but with no derivation or discussion of any physical consequences. In the perfect sink limit, we recover the mapping previously obtained with the continuum two region diffusion

model. Moreover, both kinetic rate parameters $k_{\pm}$ and P are shown independent of the field to the lowest order.

The detailed concentration profiles are not involved in the derivations of boundary conditions. The only underlying assumption is quasi-stationary condition, which is widely acceptable in studies of step dynamics. Therefore, the results obtained are expected to be generally applicable. Theoretically they can be applied directly to analyze the step dynamics in presence of a variety of driving forces, such as electric field, super or under saturation. They can be used to connect the theories and Monte Carlo simulations as we shall show later in Chapter 5.

Finally, it is worth mentioning that the results here show consistency with those from phase field models [69], while providing a simple and physically suggestive picture.

Chapter 5

Current-Induced Step Pattern Formation

5.1 Patterns of Vicinal Steps

The concept of two dimensional (2D) pattern formation by vicinal steps has been actively explored as a promising pathway for lateral nanostructuring of surfaces. Often the origin of step pattern formation is due to kinetic instabilities, developed as a result of the interplay of the fundamental physics of crystal structure and the external driving field. The typical patterns formed are step bunching and wandering.

A well-studied class of 2D pattern formation occurs for molecular beam epitaxial (MBE) growth of metal surfaces (see e.g. on Cu [70]). The basic idea can be traced to the presence of an extra energy barrier associated with the asymmetry of the step structure for adatom diffusion, known as the Ehrlich-Schwoebel (ES) barrier. Upon growth, all the steps wander in phase with a temperature and flux dependent wavelength [43]. Along the same line, Pierre-Louis *et. al.* [71] recently pointed out that another ES like asymmetry for adatom diffusion exists at kink sites, often called kink Ehrlich-Schwoebel effect (KESE). The KESE mechanism also gives rise to a 2D pattern of step wandering, although with different scaling [72].

For semiconductor surfaces like Si(111), however, there has been strong evidence for a negligible ES barrier [49, 48, 47], and conceivably not a significant KESE effect either. Part of the reason, we belive, arises from reconstruction or rebonding often occurred on semiconductor surfaces, especially near a step since there are more dangling bonds. The surface reconstruction or rebonding in general tend to diminish any asymmetry near a step.

However, based on the discussions in Chapter 2 and 3, it is clear that 2D patterning on Si surfaces can be conveniently controlled by direct current heating. It has been thoroughly discussed that the fundamental instability mechanism involves the sign of the effective kinetic coefficients. This Chapter is devoted to the study of long time dynamics of the steps resulting from current-induced instabilities. First, the typical bunching and in-phase wandering patterns are carried out by integrating the step velocity functions. Then, for some intricate step patterns recently seen in experiments where each individual step develops overhangs on itself [73], we employ a geometric approach to capture the pattern formation. Finally, 2D kinetic Monte Carlo simulations on a Solid-on-Solid (SOS) model [74] are performed. In particular, we investigated several interesting microscopic mass transport scenarios that can give rise to different instability regimes when a constant field is applied.

5.2 Velocity Function Calculation

To calculate the long time morphology of vicinal surfaces, effective equations relating the velocity of a step to the local terrace widths have proved to be very useful [75]. A simple example of such a velocity function is given by Eq. (2.9). The *extended velocity function formalism* [37, 76] takes into account also the capillarity of steps (line tension effects) as well as step repulsions, which are needed to prevent step overhangs as the initial instabilities grow. Here we also incorporate a periphery diffusion term, the sharp step analog of the parallel diffusion flux in the two-region

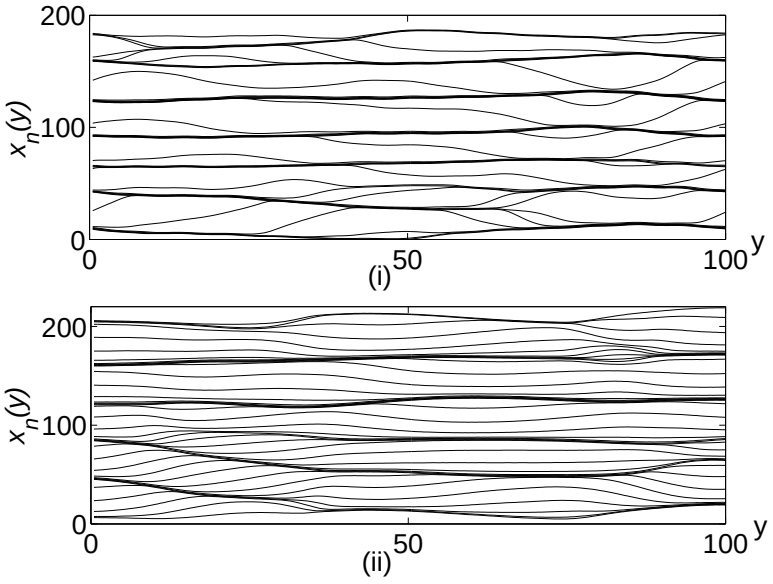

Figure 5.1: A uniform step train composed of 30 steps with spacing of $l = 10$ forms step bunches at later times both for (i) $f > 0, R > 1$ and (ii) $f < 0, R < 1$.

model. Thus the general form of the velocity function can be written as:

$$v_n(y) = f_+ \left(l_n; \mu_n, \mu_{n+1}\right) + f_- \left(l_{n-1}; \mu_{n-1}, \mu_n\right) - \partial_\tau \mathbf{J}_s \tag{5.1}$$

where $l_n(y)$ is the local width of terrace n that is in front of step n and $\mu_n(y)$ is the local chemical potential of step n.

The velocity functions $f_\pm$ contains contributions both from driven fluxes on the two neighboring terraces given by the sharp step equivalence of Eq. (2.9), and equilibrium relaxation terms that can be calculated in terms of the step edge chemical potentials μ_n [77]. The μ_n take account of both capillary effects for an individual step (using a linear approximation for the curvature) and the effects of nearest neighbor step interactions as described earlier. See Refs. [37, 76] for detailed expressions for $f_\pm$ and μ_n.

Numerically integrating Eq. (5.1), we find step bunching patterns for two parameter regimes (i) $f > 0$, $R > 1$ and (ii) $f < 0$, $R < 1$, in agreement with predictions of linear stability analysis. The bunching patterns in these two regimes

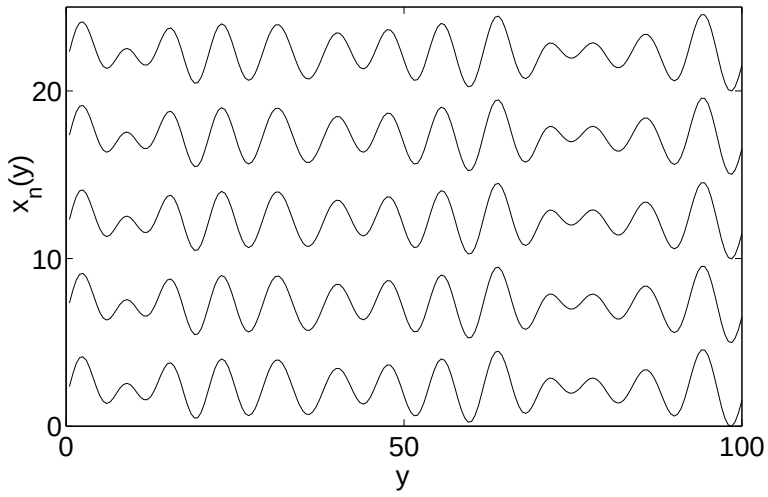

Figure 5.2: A uniform step train comprised of 5 steps with spacing $l = 5$ forms in-phase wandering patterns at later times for $f > 0, R < 1$. Notice there are some defects in the pattern because the wandering wavelength is incommensurate with the finite size of our system in the y-direction.

are qualitatively similar, as shown in Fig. 5.1. In both cases, step bunches form and grow. In between the step bunches there are crossing steps traveling from one bunch to the other.

In-phase step wandering is also given by Eq. (5.1) in the regime $f > 0$, $R < 1$, as suggested by the previous linear stability analysis. Typical wandering patterns with model parameters are shown in Fig. 5.2. Even though this is known to be a linear instability, numerically we observe that it acts very much like a nucleation process. The steps fluctuate randomly as if the surface were completely stable until a sinusoidal perturbation of the right wavelength forms. Once formed, these small scale sinusoidal waves propagate through effective "pulling" by capillary effects in the lateral direction and by step repulsions in the normal direction, until the entire surface is covered. This is qualitatively consistent with experimental findings on Si(111) [31].

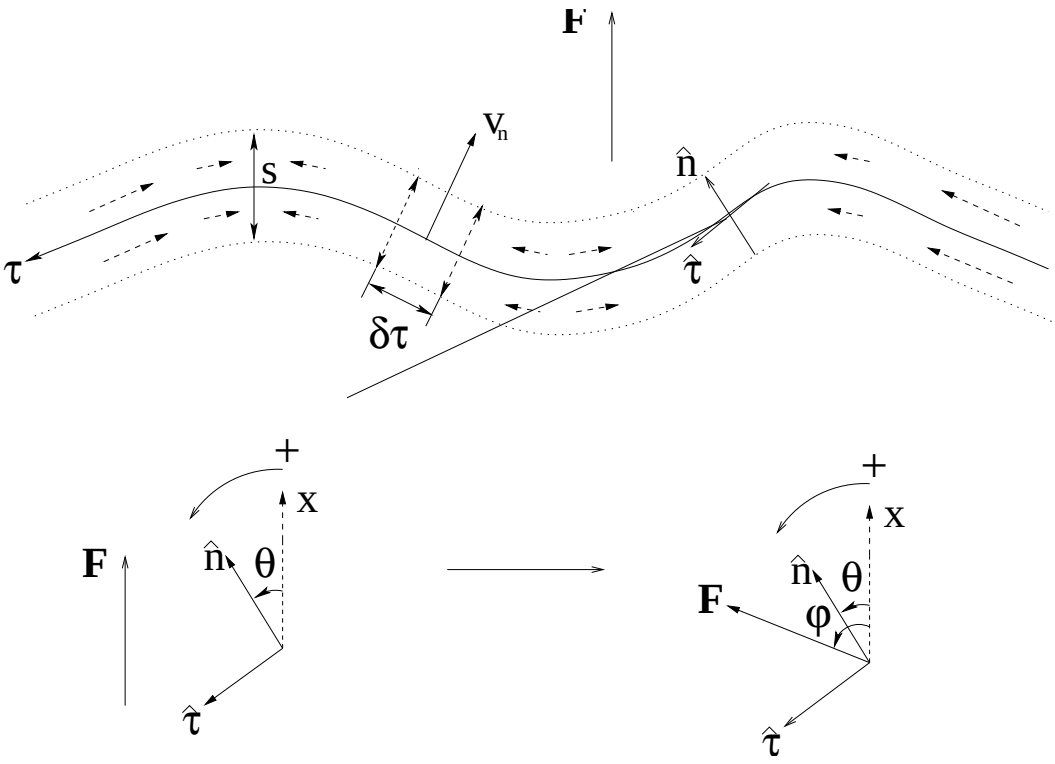

Figure 5.3: A geometrical view of a single wandering step region. The dashed arrows inside the step region schematically shows the driven flux that is parallel to the step for a step-down (x direction) field. The lower right corner shows the case when the field is at an angle φ off the x-axis.

5.3 Step Wandering in a Geometric Representation

Although Eq. (5.1) has captured many physical features, it uses a linearized curvature approximation and cannot be trusted when the step curvature becomes large. Recent experiments show a continuous distortion of the sinusoidal wandering wave by a field directed at an angle to the step normal. We treat this problem here using a geometrical representation [78, 79] of the step, where a single curve is parameterized by intrinsic properties like its arc length τ and curvature κ.

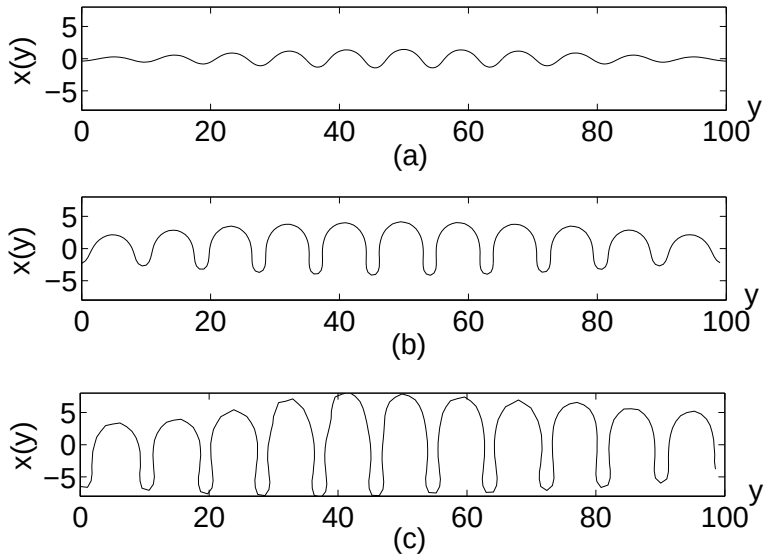

Figure 5.4: Step evolution under a perpendicular electric field (a) At $t = 160$, a linear instability develops; (b) At $t = 170$, asymmetry between the peaks and valleys creates a periodic cellular structure; (c) At $t = 190$, the cellular shape is preserved but it grows in amplitude.

5.3.1 Derivation of Equations of Motion

It suffices to concentrate on a single step, since step wandering occurs in phase. Consider a geometric representation of our step region with constant width s, as in Fig. 5.3. The morphology of the step region is specified by the position vector $\mathbf{x}(t, \tau)$ of the atomic step in the middle, where τ represents the arc length measured from an arbitrary origin. To follow $\mathbf{x}(t, \tau)$ at a later time we need to know the velocity of the curve

$$\frac{\partial \mathbf{x}}{\partial t} = v_n \hat{n} + v_\tau \hat{\tau}, \tag{5.2}$$

where $\hat{n}$ and $\hat{\tau}$ denote normal and tangential directions as before.

A general treatment of time-dependent curvilinear coordinates [80] shows the equation of motion for the curve is

$$\frac{\partial \kappa}{\partial t} = -\left[\kappa^2 + \frac{\partial^2}{\partial^2 \tau}\right] v_n + v_\tau \frac{\partial \kappa}{\partial \tau}, \tag{5.3}$$

which is subjected to the nonlocal metric constraint

$$\frac{\partial \tau}{\partial t} = v_\tau(\tau) - v_\tau(\tau = 0) + \int^\tau v_n \kappa ds'. \tag{5.4}$$

Interpreting τ as the arc length is arbitrary and other parameterizations can be used, since only the normal velocity of the curve is physically relevant. Following previous workers [78, 79], we take advantage of this "gauge freedom" and choose the *orthogonal gauge*, where τ is chosen at each instant of time so that the interface velocity has only a normal component ($v_\tau = 0$).

Now, we need to determine the normal velocity along the step. For simplicity, we will neglect contributions from the terrace diffusion field as well as from the normal diffusion field in the step region, since it has already been shown that the wandering instability we are interested in is induced by the biased diffusion parallel to the step. In the quasi-stationary limit, the diffusion field inside the step region is stationary for any given step position. To a good approximation, it can be taken as $c_s \simeq c_s^0(1 + \Gamma\kappa)$, where $c_s^0 = c_{eq}^0 s$ is the adatom density per unit step length for straight steps.

Next we consider the time rate of change of the adatoms contained in an element of the step region with an infinitesimal length $\delta\tau$ that moves with velocity v_n as in Fig. 5.3. This balance contains contributions from the motion of the step, and from the divergence of the flux parallel to the step. The latter accounts for diffusion driven both by the field and by chemical potential variations arising from changes in step curvature. We thus have

$$\begin{aligned}\left[\frac{d}{dt}(c_s \delta\tau)\right]_n &= -\Omega^{-1} v_n \delta\tau - D_s \partial_\tau \left[f c_s \sin(\varphi - \theta)\right] \delta\tau \\ &\quad + D_s \partial_\tau^2 c_s \delta\tau.\end{aligned} \tag{5.5}$$

Using the exact geometrical relation $[d(\delta\tau)/dt]_n = v_n \kappa \delta\tau$, which can be understood physically as the rate at which the arc length $\delta\tau$ on a circle of radius $|\kappa^{-1}|$ changes

if the circle grows only radially at rate v_n, Eq. (5.5) reduces to the following form

$$\begin{aligned}\frac{v_n\left[1+\Omega c_s^0\left(1+\Gamma\kappa\right)\kappa\right]}{\Omega D_s c_s^0} &= f\cos\left(\varphi-\theta\right)\left(1+\Gamma\kappa\right)\kappa \\ &\quad -f\sin\left(\varphi-\theta\right)\Gamma\partial_\tau\kappa+\Gamma\partial_\tau^2\kappa.\end{aligned} \tag{5.6}$$

Combining Eq. (5.6) with Eqs. (5.3) and (5.4) yields a complete description of the dynamics of a single step region in the presence of an electric field at an angle φ off the x-axis.

5.3.2 Numerical Results

We first consider the special case $\varphi = 0$ where the external field is perpendicular to the average step direction (the y -axis). In Fig. 5.4, we show three step configurations evolving from a straight step with a small perturbation in the middle. The linear wandering instability develops first as shown in Fig. 5.4(a), then gradually changes into a cellular shape with the wavelength selected by the linear instability, as illustrated in Fig. 5.4(b). At later stages, the cellular shape grows without significant distortion or overlap, as shown in Fig. 5.4(c). Notice that indeed we observe numerically a long time period before the linear instability is significant.

In Fig. 5.5, we show configurations of the system with $\varphi = \pi/4$. Fig. 5.5 suggests that the linear instability is induced by the perpendicular component of the field. However, as the magnitude of the instability grows, the peaks turn gradually until they are aligned with the direction of the field. We obtain the same peak turning process when the angle φ is varied while keeping f constant. However, since the perpendicular component decreases with increasing φ, both the wavelength selected by the initial instability as in Eq. (2.11) and the time period before it forms increases monotonically with φ. The numerical results for three particular angles are shown in Fig. 5.6.

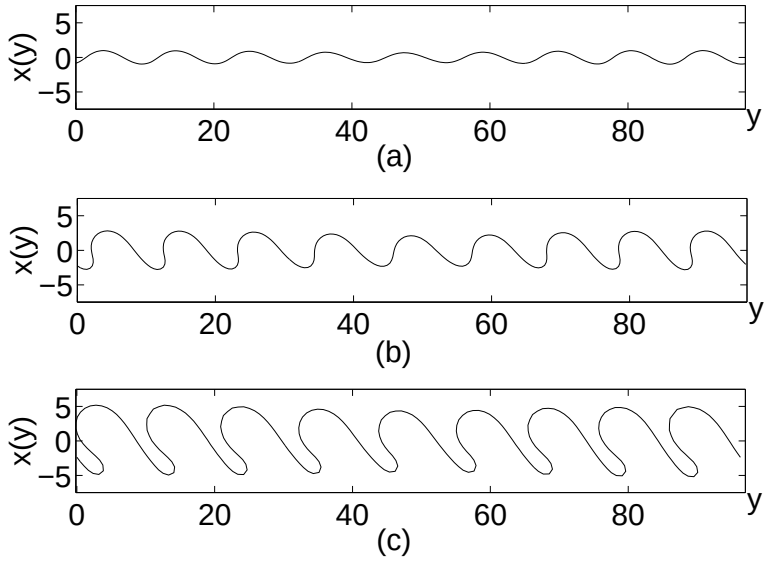

Figure 5.5: Step evolution when the electric field is at an angle $\varphi = \pi/4$ from the x-axis: (a) $t = 300$, the initial instability induced by the normal component of the field; (b) $t = 315$, the peaks have begun to turn; (c) $t = 330$, all the peaks align with the direction of the field.

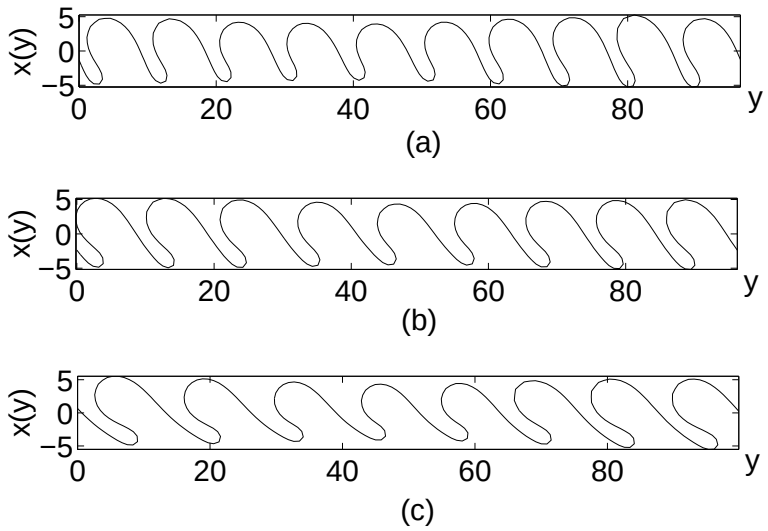

Figure 5.6: Comparison of the step evolution as the angle φ increases: (a) $t = 230$, $\varphi = \pi/6$; (b) $t = 330$, $\varphi = \pi/4$; (c) $t = 640$, $\varphi = \pi/3$.

5.3.3 Discussion

To provide a more qualitative understanding of the pattern formation process, we neglect the higher order terms in κ in Eq. (5.6). To linear order in κ, Eq. (5.6) becomes

$$\frac{v_n}{\Omega D_s c_s^0} = f\kappa\cos(\varphi-\theta) - f\sin(\varphi-\theta)\,\partial_\tau\kappa + \Gamma\partial_\tau^2\kappa. \tag{5.7}$$

In particular, for $\varphi = 0$

$$\frac{v_n}{\Omega D_s c_s^0} = f\kappa\cos\theta + f\sin\theta\partial_\tau\kappa + \partial_\tau^2\kappa. \tag{5.8}$$

In the usual Mullins-Sekerka instability κ alone appears in the first term. Here however we have $\kappa\cos\theta$, resulting from field driven diffusion inside the step region. The extra $\cos\theta$ term brings in a field induced anisotropy that makes the peaks and valleys of a perturbation preferably grow rather than the sides. This stabilizes cellular structures. This anisotropy will keep the tip unsplit, and it provides a cut off as the sides become nearly vertical. Thus the cellular shapes formed under the influence of the external field do not emit side branches, in contrast to most systems that undergo a Mullins-Sekerka instability.

The second term in Eq. (5.7) is a flux induced by $-\kappa$ that effectively transports mass from the bottom to the top of a bulge and is responsible for the asymmetric shape of the peaks and valleys, as is illustrated in Fig. 5.7.

Although Eq. (5.7) is linear in the curvature, κ itself is a highly nonlinear function of the deviation from a straight step. The early evolution is governed by the following linearized equation

$$\frac{1}{\Omega D_s c_s^0}\frac{\partial x}{\partial t} = -f\cos\varphi\frac{\partial^2 x}{\partial y^2} - f\sin\varphi\frac{\partial^3 x}{\partial y^3} - \Gamma\frac{\partial^4 x}{\partial y^4}. \tag{5.9}$$

The above equation is unstable when $f\cos\varphi > 0$, suggesting that the wavelength selection is determined by the perpendicular component of the field. For $\varphi = 0$, perturbations with wavenumber $q_0 = 1/(\sqrt{2}\xi)$ are maximally amplified. For $0 < \varphi <$

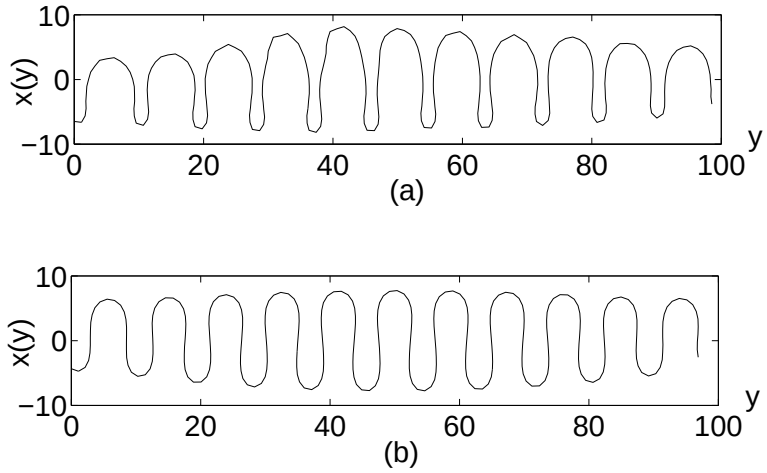

Figure 5.7: A study of the asymmetry of the cellular patterns: (a) $t = 180$, a snapshot of the system given by Eq. (5.8). Note the close agreement with Fig. 5.4(c). This shows that the simplified Eq. (5.7) with only terms linear in κ captures most features of Eq. (5.6); (b) $t = 180$, a snapshot of a model equation where the term $\sim \partial_\tau \kappa$ is left out of Eq. (5.8). Clearly this term is mainly responsible for the asymmetric shape in (a).

$\pi/2$, the most unstable wavenumber selected by the linear instability is decreased by a factor of $\sqrt{\cos\varphi}$, i.e., $q_\varphi = q_0\sqrt{\cos\varphi}$.

As the instability grows, the field induced anisotropy characterized by the factor $\cos(\varphi-\theta)$ becomes more significant. As in the $\varphi = 0$ case above, the anisotropy makes the initial sinusoidal wave grows preferably in the direction where $\cos(\varphi-\theta)$ in Eq. (5.7) attains its minimum. Thus the wave will be continuously distorted until the peaks point toward the field direction, and subsequently only the magnitude of the pattern grows.

5.4 Monte Carlo Simulations

A quantitative Monte Carlo calculation of a full 2D atomistic diffusion model under external driving force would be extremely hard, and it would be almost impossible to simulate the long time behavior of the system with real world parameters. Fortunately, as we demonstrated previously in Section 5.2, our hope of predicting the long time dynamics comparable to experiments is achieved quite well by mesoscopic velocity function calculations.

Nevertheless, it is useful to generate a computationally simple Monte Carlo scheme that takes account of the microscopic physics of both the positive and negative kinetic coefficients in a reasonable way. This becomes quite easy to do since we have already established a general mapping scheme from discrete hopping to continuum modeling and vice versa. Moreover, based on the mapping one can easily explore using simulations a host of possible boundary conditions that may be relevant for other surfaces, in particular the asymmetric cases such as ES or inverse ES. These studies will shed light on the understanding of negative kinetic coefficient and the generality of current-induced instability mechanism.

5.4.1 SOS Model with Biased Diffusion

The study here is based on a 2D SOS system - in which the surface is represented by a discrete height function of columns of atoms - under the influence of an external driving force. The SOS model in general belongs to the broad class of 'broken bond models', in which the total energy is assumed to be proportional to the number of bonds between neighboring columns. We believe that this is the simplest microscopic model that can properly describes the interplay between adatom diffusion and step motion. Unlike the velocity function calculations where we focus on the step motion from the very beginning by coarse graining the surface, the spirit of the SOS model is to obtain the large scale dynamics from purely individual atomic motions.

Restricted to only nearest neighbor interactions, the Hamiltonian of a general SOS system can be written as

$$H = \sum_{<ij>} \epsilon \left| h_i - h_j \right| \tag{5.10}$$

where h_i is the height of column i and $< ij >$ denotes the nearest neighbor pairs. 2ϵ is the energy associated with each broken bond. The total energy clearly depends on lattice structure. However, without losing any interesting physics, we will confined ourselves to a square lattice for simplicity. Thus the transition probability from state i to j, i.e. the probability for an atom hopping from site i to its nearest neighbor site j, is simply

$$\Gamma_{i \to j} \propto \exp\left(-2\epsilon n_i\right), \tag{5.11}$$

where $n_i = 0, ..., 4$, is the number of the nearest neighbor bonds that the atom at site i has.

The external electric field induces small effective charges and thus exerts constant forces on atoms. Neglect the small atomic masses, the adatoms undergo driven diffusion with constant drift velocity. This can be simulated by putting a bias on diffusion parallel to the current direction, which favors motion along the current direction by a factor of $\exp(2\left|\mathbf{F}\right| a/k_B T)$ when compared to the opposite direction. We

always assume positive effective charge here, and the motion that is perpendicular to the field direction is assumed not affected.

5.4.2 Simulating a *Negative* Kinetic Coefficient

In previously proposed theory, the current-induced instabilities depend on the sign of the kinetic coefficients for a given current direction, which in turn originated from the relative diffusion rate between on terrace and near a step. It may seem difficult to implement the different diffusion rates using such an atomistic model, simply because there are no explicitly defined "steps" or "terraces" except as initial conditions. To solve this problem, we adopt the scheme of *modified Arrhenius dynamics*, suggested by Liu and Weeks in the study of electromigration on Si(111) at temperature range I [35]. The basic idea is that the energy difference between the two states before and after the move tells important information about the local structure, so that one can use it to effectively distinguish the adatom motion on terraces and near a step.

To a good approximation, if the adatom movement does not change the energy, it corresponds to adatom diffusion on the "terrace" region, while a change in energy results from attachment/detachment at a step. The approximation relies on the fact that there is no significant island nucleation processes occurring, since the adatom concentration is generally low on terraces in both experimental and our simulation regime. Note that the step region that we constructed in this way always has a constant width of $2a$.

In their work, Liu and Weeks impose an *extra barrier* for adatom attachment/detachment, which originated from the physics of step reconstruction. This corresponds to a positive effective kinetic coefficient. Here, we shall study the case of the negative kinetic coefficient simply by imposing the extra barrier on terrace

diffusion. In particular, the transition rate between state i and j is constructed as

$$\Gamma_{i\to j} = \begin{cases} \exp(-2\epsilon n_i), \triangle E_{ij} \neq 0 \\ b\exp(-2\epsilon n_i), \triangle E_{ij} = 0 \end{cases} \tag{5.12}$$

where $b < 1$ denotes the extra diffusion barrier on terrace diffusion.

The initial configuration of the simulation is a uniformly stepped surface containing 30 single atomic height steps that run along the y direction, and a large diffusion bias is put along x direction with $|f| = |\mathbf{F}|/k_BT = .2$. During the simulation, $b = 0.1$ and $\epsilon/k_BT = 1$ are assumed. It should be mentioned that much narrower terrace and stronger field than reality are chosen here to speed up the simulation. This is appropriate since we are not interested in any quantitative detail here, rather the qualitative idea of current-induced instabilities and the association between the kinetic coefficients and microscopic hopping rates. Two snapshots of the system for negative kinetic coefficient but with $f > 0$ and $f < 0$ are shown in Fig. 5.8 and Fig. 5.9, respectively. In addition, the system is completely stable when $b = 1$ as we expected, since all the steps are at local equilibrium.

5.4.3 Asymmetric Kinetic Coefficients

In the theory of current-induced instabilities for Si surfaces, only symmetric kinetic coefficients are considered due to the unimportance of the ES barrier in general on semiconductor surfaces. However, the ES barrier is proved to exist on many other surfaces and plays an important role in surface morphology under non equilibrium driving (see discussion in Section 5.1), most commonly studied with growth flux or sublimation. With the knowledge of the ES barrier that has been extensively discussed in the past decade and the surface electromigration that we believe to have a good understanding of, it seems natural to explore the interplay of the two, which has not been addressed in the literature.

Still we follow the basic idea of modified Arrhenius dynamics, and try to impose an energy barrier for adatom motion of descending steps. Obviously the

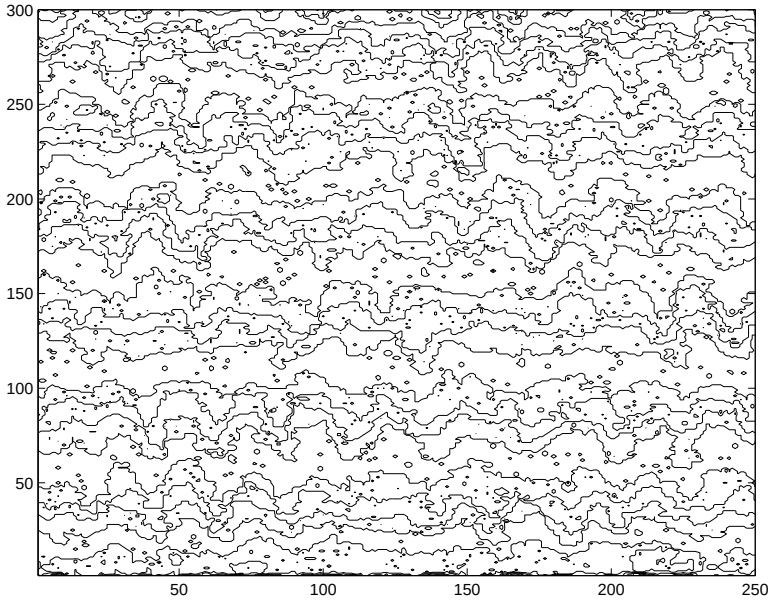

Figure 5.8: Monte Carlo simulation in the case of $d < 1$ and $q > 0$, with an initial step train containing 30 steps of uniform spacing $l = 10$.

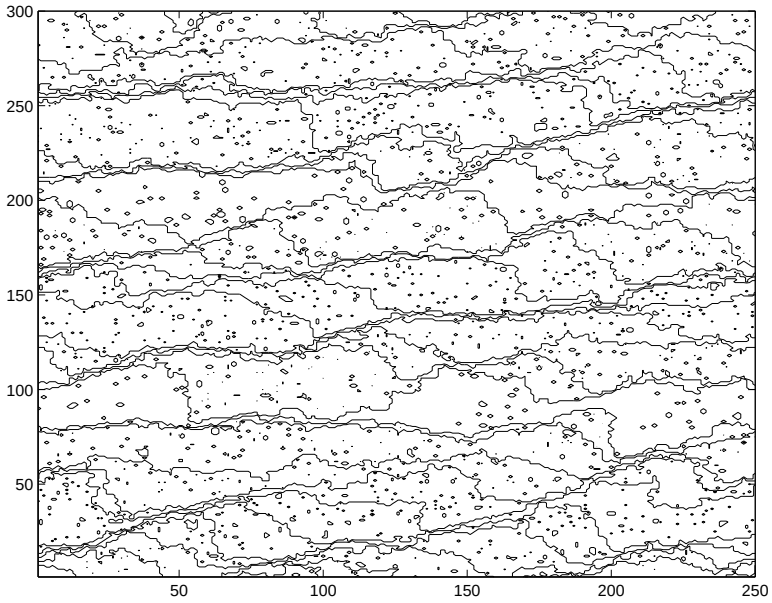

Figure 5.9: Monte Carlo simulation in the case of $d < 1$ and $q < 0$, with an initial step train containing 30 steps of uniform spacing $l = 10$.

energy measure that are used previously becomes inappropriate in this case, since the energy difference is symmetric on the two sides of the step. Instead we shall use the column height as our new measure. In an SOS model, an atom at site i hopping to one of its nearest neighbor site j is simulated by changing height of column i and j with one unit in the opposite way ($h_i \to h_i - 1$ and $h_j \to h_j + 1$). Hence, if we define our measure to be $\triangle h_{ij} = h_i - h_j$, all the diffusion process on the same terrace satisfy $\triangle h_{ij} \equiv 1$, whereas an atom hopping from one terrace to the other at a step edge is associate with $\triangle h_{ij} \neq 1$. Note that no permeability or multi-site jumps are allowed in this model. Of course, there are some other possible events on the surface with $\triangle h_{ij} \neq 1$, such as creation of adatom vacancy or adatom overhang, but these are very low probability events and can be neglected to a good approximation. Therefore, the transition rate for an atom hopping from site i to its nearest neighbor site j takes the form

$$\Gamma_{i\to j} = \begin{cases} \exp(-2\epsilon n_i), \triangle h_{ij} = 1 \\ b\exp(-2\epsilon n_i), \triangle h_{ij} \neq 1 \end{cases} \tag{5.13}$$

in which everything is as previously defined.

Using the transition rate defined as in Eq. (5.13), the SOS system is simulated with the same initial conditions as in the previous section. Interestingly, it is found that there is always stable step flow in case of $f < 0$, while big step bunches and large terraces form in the case of $f > 0$, as is shown in Fig. 5.10.

The result here can be understood as the following. First of all, notice that the system with diffusion property defined by Eq. (5.13) generates a special case of ES barrier. On the lower side of the step, the attachment rate is the same as terrace diffusion. Hence the effective kinetic coefficient diverges and the step is at local equilibrium on this side ($k_+ \to \infty$ or $d_+ \to 0$). On the other side, the rate of descending step is very low compared to terrace diffusion. Hence a finite and positive kinetic coefficient ($k_- > 0$) is generated. Second, in presence of step asymmetry, the current-induced instabilities in general depend on the factor $f(d_+ + d_-)$. Therefore

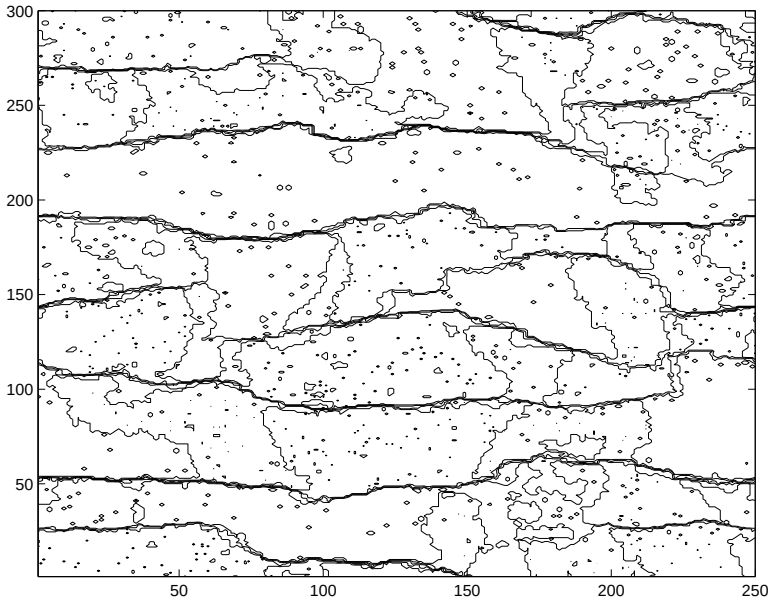

Figure 5.10: Monte Carlo simulation in the case of $d > 1$ and $q > 0$, with an initial step train containing 30 steps of uniform spacing $l = 10$.

the instability will occur in a similar fashion as Si(111) in temperature range I or Si(001) with step-down current.

Combining the energy and height measure, another interesting case can be simulated with transition rate

$$\Gamma_{i\to j} = \begin{cases} \exp(-2\epsilon n_i), \triangle h_{ij} = 1 \text{ and } \triangle E_{ij} \neq 0 \\ b\exp(-2\epsilon n_i), \text{ otherwise} \end{cases} \tag{5.14}$$

Note that this is a case in which the attachment/detachment from the lower side of the step is much faster than anything else. In this case, the effective kinetic coefficient on the upper side of the step diverges ($k_- \to \infty$ or $d_- \to 0$), while a negative kinetic coefficient is generated on the lower side of the step. The instabilities are therefore expected to be the same as the temperature range II on Si(111) or Si(001) with a step-up current. The simulation results confirm the reasoning here and resemble the patterns in Fig. 5.8-5.9.

Other models can also be created by tuning the three rate parameters distin-

guished by some combination of height and energy measures. All the results are consistently interpreted with the theory previously developed in the similar way as above.

Chapter 6

Conclusion

This chapter summarizes the main contributions in this dissertation, and conclude with possible directions for future work.

The first basic idea introduced is to allow for different diffusion pathways on terraces and in a small region around a step in models of step dynamics. The idea is physically plausible and is motivated by surface rebonding or reconstruction that are likely important on semiconductor surfaces. In the thesis we examine the consequences of the simplest realization of this idea, in which isotropic diffusion in both regions and fixed width for step regions are assumed. The key parameter in the model is the relative diffusivity that in general depends on temperature. The steady state of this simple two region model is suggestive, in that it provides a physical way of understanding both bunching and wandering instabilities plus a plausible transition mechanism with temperature.

The second key idea is to use extrapolation of the two region results to relate the effective kinetic boundary conditions to microscopic physical processes. Using extrapolation to obtain sharp step boundary conditions is new for this field and it elucidates the physical meaning of the effective parameters. The idea is applied first to the two region diffusion model, where we extrapolate the concentration profiles on terraces to obtain the linear kinetics boundary condition. Through the mapping, it is

found that the lowest order result is independent of the field, in contrast to previous suggestions by other researchers. Moreover, for the first time to our knowledge, the negative kinetic coefficient is connected to plausible physical processes.

The idea of extrapolation can be applied more generally as is shown in the study of the 1D hopping model. Without assuming much detailed information about the physical processes on terraces, we are able to derive the general linear kinetics boundary conditions using the quasi-stationary approximation. The derivation is simpler and can be easily interpreted in a physical context when compared to the much involved derivation from phase field models [69]. The results directly relate the microscopic parameters in kinetic Monte Carlo simulations to the effective parameters in a generalized sharp step model.

The third idea is to introduce a geometric representation of the step to elucidate some nonlinear features of step patterns seen in step wandering instabilities. A geometrical representation which uses arclength and curvature to parameterize a 2D curve is not new and has proven very useful in dendritic growth problems [78, 79]. In the dissertation, we adopt this representation to derive the highly nonlinear evolution equations for current-induced step wandering. The advantage of the geometric approach is that it does not introduce any artificial restrictions on the resulting shapes, in contrast to the usual $x(y)$ representation, where x is assumed to be a single valued function of y. Thus it allows us to describe step patterns with large curvature and even "overhangs" that can not be captured by the standard multi-scale expansion method [81, 82].

Guided by the above conceptual ideas, we have obtained a number of new results in terms of instabilities and patterns. We proposed a coherent scenario for temperature dependent current-induced instabilities on Si(111), and analyze the step bunching in both current directions through step pairing on Si(001). Based on these, a unified view of current-induced instabilities is formulated in terms of the sign of kinetic coefficients. We also extended the velocity function formalism to

include both negative kinetic coefficients and periphery diffusion, so that the bunching and in-phase step wandering patterns for Si(111) at middle temperatures can be carried out. The nonlinear peak turning pattern has been described well by the numerical solutions of the geometric equations. Moreover, some interesting Monte Carlo simulations are studied, not only to implement the general mapping results from the hopping model, but also put the theory of current-induced instabilities in a more general context where step asymmetry is also considered.

Going forward, there are several directions to pursue. First, we can do further study of the instabilities on Si(111) in middle temperature range. In particular, it will be interesting and reasonably straightforward to take sublimation and supersaturation explicitly into account, especially since recently there seems to be some controversy about whether the growth flux can change the unstable current direction [83, 84]. Moreover, a study of scaling and relaxation in this regime, which could differ from the commonly studied regime of positive kinetic coefficients, seems worthwhile. Second, it is possible to extend the 1D hopping model to 2D, and thus gain a better understanding of the periphery diffusion term in the sharp step boundary condition from the physically motivated picture of the two region diffusion model. Third, it might be possible to generalize the geometric single step approach for in phase step wandering to account in an effective way for repulsion from other steps. This could better describe cases where adjacent steps are close together. More generally, we expect continuing experimental and theoretical work on driven instabilities on surfaces as workers try to understand and exploit the interesting patterns that emerge.

LIST OF FIGURES

LIST OF TABLES

BIBLIOGRAPHY

[1] E. E. Gruber and W. W. Mullins. *J. Phys. Chem. Solids*, 28:875, 1967.

[2] C. Jayaprakash, C. Rottman, and W. F. Saam. *J. Phys. Chem. Solids*, 28:875, 1967.

[3] E. D. Williams, R. J. Phaneuf, J. Wei, N. C. Bartelt, and T. L. Einstein. *Surf. Sci.*, 310:451, 1994.

[4] J. D. Weeks. *Ordering in Strongly Fluctuating Condensed Matter Systems*, page 293. Plenum, New York, 1980.

[5] S. T. Chui and J. D. Weeks. *Phys. Rev. B*, 14:4978, 1976.

[6] P. Nozières and F. Gallet. *J. de. Physique*, 48:353, 1987.

[7] G. J. Shiflet and J. van der Merwe. *Surf. Sci.*, 256:187, 1991.

[8] J. van der Merwe and G. J. Shiflet. *Surf. Sci.*, 256:171, 1991.

[9] M. D. Thompson and H. B. Huntington. *Surf. Sci.*, 116:522, 1982.

[10] J. Krug. *Physica A*, 313:47, 2002.

[11] S. P. Garcia, H. Bao, and M. A. Hines. *J. Phys. Chem. B*, 108:6062, 2004.

[12] K. Yagi, H. Minoda, and M. Degawa. *Surf. Sci. Rep.*, 43:45, 2001.

[13] L. I. Rubenstein. *The Stefan Problem*. AMS, Providence, Rhode Island, 1971.

[14] A. M. Meirmanov. *The Stefan Problem*. W. de Gruyter, Berlin, 1992.

[15] J. J. Clement, A. S. Oates, R. Rosenberg, and P. M. Lenahan. *Materials Reliability in Microelectronics VI*, page p.81. Material Research Society, Pittsburgh, PA, 1996.

[16] J. R. Lloyd and J. J. Clement. *Thin Solid Film*, 262:135, 1995.

[17] A. V. Latyshev, A. L. Aseev, A. B. Krasilnikov, and S. I. Stenin. *Surf. Sci.*, 213:157, 1989.

[18] Y. Homma, R. I. McClelland, and H. Hibino. *Jpn. J. Appl. Phys.*, 29:L2254, 1990.

[19] Y. Homma and M. Suzuki. *Appl. Surf. Sci.*, 60/61:479, 1992.

[20] M. Suzuki, Y. Homma, Y. Kudoh, and R. Kaneko. *Appl. Surf. Sci.*, 60/61:460, 1992.

[21] H. Tokumoto and M. Iwatsuki. *Jpn. J. Appl. Phys.*, 32:1368, 1993.

[22] H. Tokumoto, K. Miki, Y. Morita, T. Sato, M. Iwatsuki, M. Suzuki, and T. Fukuda. *Ultramicroscopy*, 42-44:816, 1992.

[23] M. J. Ramstad, R. J. Birgeneau, K. I. Blum, and D. Y. Noh. *Europhys. Lett.*, 24:653, 1993.

[24] E. D. Williams, E. Fu, Y.-N Yang, D. Kandel, and J. D. Weeks. *Surf. Sci.*, 336:L746, 1995.

[25] Y.-N Yang, E. Fu, and E. D. Williams. *Surf. Sci.*, 356:101, 1996.

[26] E. Fu, D.-J. Liu, M. D. Johnson, J. D. Weeks, and E. D. Williams. *Surf. Sci.*, 385:259, 1997.

[27] N. Osakabe, Y. Tanishiro, K. Yagi, and G. honjo. *Surf. Sci.*, 109:353, 1981.

[28] W. Telieps and E. Bauer. *Surf. Sci.*, 162:163, 1985.

[29] M. Degawa, H. Minoda, Y. Tanishiro, and K. Yagi. *Surf. Rev. Lett.*, 6:977, 1999.

[30] M. Degawa, H. Nishimura, Y. Tanishiro, H. Minoda, and K. Yagi. *Jpn. J. Appl. Phys.*, 38:L308, 1999.

[31] M. Degawa, K. Thüermer, I. Morishima, H. Minoda, K. Yagi, and E. D. Williams. *Surf. Sci.*, 487:171, 2001.

[32] W. K. Burton, N. Cabrera, and F. C. Frank. *Proc. R. Soc. London A*, 243:299, 1951.

[33] S. Stoyanov. *Jpn. J. Appl. Phys.*, Part 1 30:1, 1991.

[34] S. Stoyanov, H. Nakahara, and M. Ichikawa. *Jpn. J. Appl. Phys.*, 33:254, 1994.

[35] D.-J. Liu and J. D. Weeks. *Phys. Rev. B*, 57:14891, 1998.

[36] D. Kandel and E. Kaxiras. *Phys. Rev. Lett.*, 76:1114, 1996.

[37] D.-J. Liu, J. D. Weeks, and D. Kandel. *Surf. Rev. Lett.*, 4:107, 1997.

[38] K. Thüermer, D.-J. Liu, E. D. Williams, and J. D. Weeks. *Phys. Rev. Lett.*, 83:5531, 1999.

[39] M. Degawa, H. Minoda, Y. Tanishiro, and K. Yagi. *Surf. Sci.*, 461:L528, 2000.

[40] S. Stoyanov. *Surf. Sci.*, 416:200, 1998.

[41] M. Sato, M. Uwaha, and Y. Saito. *Phys. Rev. B*, 39:4412, 2000.

[42] N. Suga, J. Kimpara, N.-J. Wu, H. Yasunaga, and A. Natori. *Jpn. J. Appl. Phys.*, 39:4412, 2000.

[43] G. S. Bales and A. Zangwill. *Phys. Rev. B*, 41:5500, 1990.

[44] G. S. Bales and A. Zangwill. Erratum. *Phys. Rev. B*, 48:2024, 1993.

[45] W. W. Mullins and R. F. Sekerka. *J. Appl. Phys.*, 34:323, 1963.

[46] W. W. Mullins and R. F. Sekerka. *J. Appl. Phys.*, 35:444, 1964.

[47] A. Pimpinelli, J. Villain, D. E. Wolf, J. J. Métois, J. C. Heyraud, I. Eikinani, and G. Ulmin. *Surf. Sci.*, 295:143, 1993.

[48] A. Ichimiya, Y. Tanaka, and K. Ishiyama. *Phys. Rev. Lett.*, 76:4721, 1996.

[49] H. Hibino, C.-W. Hu, T. Ogino, and I.S.T. Tsong. *Phys. Rev. B*, 63:245402, 2001.

[50] K. Binder and P. C. Hohenberg. *Phys. Rev. B*, 6:3461, 1972.

[51] P. Politi and J. Villain. *Phys. Rev. B*, 54:5114, 1996.

[52] S. D. Cohen, R. D. Schroll, T. L. Einstein, J.-J. Métois, H. Gebremariam, and H. L. Richards E. D. Williams. *Phys. Rev. B*, 66:115310, 2002.

[53] T. Doi, M. Ichikawa, and S. Hosoki. *Phys. Rev. B*, 55:1864, 1997.

[54] A. V. Latyshev, L. V. Litvin, and A. L. Aseev. *Appl. Surf. Sci.*, 130-132:139, 1998.

[55] H. J. W. Zandvliet. *Rev. Mod. Phys.*, 72:593, 2000.

[56] Y. W. Mo and M. G. Lagally. *Surf. Sci.*, 248:313, 1991.

[57] J.-F. Nielsen, M. S. Pettersen, and J. P. Pelz. *Surf. Sci.*, 480:84, 2001.

[58] J. Mysliveček, C. Schelling, F. Schäffler, G. Springholz, P. Šmilauer, J. Krug, and B. Voigtländer. *Surf. Sci.*, 520:193, 2002.

[59] A. Natori, H. Fujimura, and H. Yasunaga. *Jpn. J. Appl. Phys.*, 31:1164, 1992.

[60] D.-J. Liu, J. D. Weeks, and D. Kandel. *Phys. Rev. Lett.*, 81:2743, 1998.

[61] M. Sato, M. Uwaha, Y. Saito, and Y. Hirose. *Phys. Rev. B*, 65:245427, 2002.

[62] H.-C. Jeong and E. D. Williams. *Surf. Sci. Repts*, 34:171, 1999.

[63] A. A. Chernov. *Sov. Phys. Crystallog.*, 1:88, 1956.

[64] A. A. Chernov. *Sov. Phys. Uspekhi.*, 4:116, 1961.

[65] G. Ehrlich and F. Hudda. *J. Chem. Phys.*, 44:1039, 1966.

[66] R. L. Schwoebel. *J. Appl. Phys.*, 40:614, 1969.

[67] M. Ozdemir and A. Zangwill. *Phys. Rev. B*, 45:3718, 1992.

[68] R. Ghez and S. S. Iyer. *IBM J. Res. Develop.*, 32:804, 1988.

[69] O. Pierre-Louis. *Phys. Rev. E*, 68:021604, 2003.

[70] L. Schwenger, R. Folkerts, and H. J. Ernst. *Phys. Rev. B*, 55:R7406, 1997.

[71] O. Pierre-Louis, M. R. D'Orsogna, and T. L. Einstein. *Phys. Rev. Lett.*, 82:3661, 1998.

[72] J. Kallunki, J. Krug, and M. Kotrla. *Phys. Rev. B*, 65:205411, 2002.

[73] M. Degawa, H. Minoda, Y. Tanishiro, and K. Yagi. *Phys. Rev. B*, 63:045309, 2001.

[74] M. Siegert and M. Plischke. *Phys. Rev. E*, 50:917, 1994.

[75] P. Bennema and G. H. Gilmer. *Crystal Growth: An Introduction*, page 263. North Holland, Amsterdam, 1973.

[76] J. D. Weeks, D.-J. Liu, and H.-C. Jeong. *Dynamics of crystal surfaces and interfaces*, pages 199–216. Plenum, New York, 1997.

[77] D.-J. Liu, E. S. Fu, M. D. Johnson, and J. D. Weeks E. D. Williams. *J. Vac. Sci. Tech. B*, 14(4):2799, 1996.

[78] R. C. Brower, D. A. Kessler, J. Koplik, and H. Levine. *Phys. Rev. Lett.*, 51:1111, 1983.

[79] R. C. Brower, D. A. Kessler, J. Koplik, and H. Levine. *Phys. Rev. A*, 51:1111, 1983.

[80] J. D. Weeks and W. van Saarloos. *Phys. Rev. A*, 35:3001, 1987.

[81] I. Bena, C. Misbah, and A. Valance. *Phys. Rev. B*, 47:7408, 1993.

[82] O. Pierre-Louis, C. Misbah, Y. Saito, J. Krug, and P. Politi. *Phys. Rev. Lett.*, 80:4221, 1998.

[83] J. J. Métois and S. Stoyanov. *Surf. Sci.*, 440:407, 1999.

[84] B. J. Gibbons, J. Noffsinger, and J. P. Pelz. *unpublished.*